Report

Current Biology

Memory encoding and retrieval by retrosplenial parvalbumin interneurons are impaired in Alzheimer's disease model mice

Highlights

- Memory-encoding RSC PV neuron population decreases in 5XFAD mice
- Upregulated PV neuron dynamics during memory retrieval are disrupted in 5XFAD mice
- Memory-induced potentiation of the PV neuron synapse is impaired in 5XFAD mice
- Optogenetic activation of PV neurons restores memory retrieval in 5XFAD mice

Authors

Kyerl Park, Michael M. Kohl, Jeehyun Kwag

Correspondence

jkwag@snu.ac.kr

In brief

How memory is represented in GABAergic interneurons and how their dysfunction relates to memory deficits in Alzheimer's disease (AD) are unknown. Park et al. report that the synaptic dysfunction of retrosplenial PV interneurons in 5XFAD mice disrupts the ensemble dynamics underlying memory encoding and retrieval, leading to memory deficits in AD.

Park et al., 2024, Current Biology *34*, 1–10
January 22, 2024
https://doi.org/10.1016/j.cub.2023.12.014

CellPress

Current Biology

CellPress
OPEN ACCESS

Report

Memory encoding and retrieval by retrosplenial parvalbumin interneurons are impaired in Alzheimer's disease model mice

Kyerl Park,[1,2] Michael M. Kohl,[3] and Jeehyun Kwag[1,4,5,*]
[1]Department of Brain and Cognitive Sciences, Seoul National University, Gwanak-ro 1, Gwanak-gu, Seoul 08826, Korea
[2]Department of Brain and Cognitive Engineering, Korea University, Anam-ro 145, Seongbuk-gu, Seoul 02841, Korea
[3]School of Psychology and Neuroscience, University of Glasgow, University Avenue, Glasgow G12 8QQ, UK
[4]X (formerly Twitter): @jkwag_nclab
[5]Lead contact
*Correspondence: jkwag@snu.ac.kr
https://doi.org/10.1016/j.cub.2023.12.014

SUMMARY

Memory deficits in Alzheimer's disease (AD) show a strong link with GABAergic interneuron dysfunctions.[1–7] The ensemble dynamics of GABAergic interneurons represent memory encoding and retrieval,[8–12] but how GABAergic interneuron dysfunction affects inhibitory ensemble dynamics in AD is unknown. As the retrosplenial cortex (RSC) is critical for episodic memory[13–16] and is affected by β-amyloid accumulation in early AD,[17–21] we address this question by performing Ca^{2+} imaging in RSC parvalbumin (PV)-expressing interneurons during a contextual fear memory task in healthy control mice and the 5XFAD mouse model of AD. We found that populations of PV interneurons responsive to aversive electric foot shocks during contextual fear conditioning (shock-responsive) significantly decreased in the 5XFAD mice, indicating dysfunctions in the recruitment of memory-encoding PV interneurons. In the control mice, ensemble activities of shock-responsive PV interneurons were selectively upregulated during the freezing epoch of the contextual fear memory retrieval, manifested by synaptic potentiation of PV interneuron-mediated inhibition. However, such changes in ensemble dynamics during memory retrieval and synaptic plasticity were both absent in the 5XFAD mice. Optogenetic silencing of PV interneurons during contextual fear conditioning in the control mice mimicked the memory deficits in the 5XFAD mice, while optogenetic activation of PV interneurons in the 5XFAD mice restored memory retrieval. These results demonstrate the critical roles of contextual fear memory-encoding PV interneurons for memory retrieval. Furthermore, synaptic dysfunction of PV interneurons may disrupt the recruitment of PV interneurons and their ensemble dynamics underlying contextual fear memory retrieval, subsequently leading to memory deficits in AD.

RESULTS

Encoding of contextual fear memory by RSC PV interneurons is impaired in 5XFAD/PV-Cre mice

Neurons in the retrosplenial cortex (RSC) have been suggested to encode contextual fear memory.[14,15] Distinct subtypes of GABAergic interneurons in multiple neural circuits have been reported to play key roles in memory functions.[8–12] However, the roles of RSC parvalbumin (PV)-expressing interneurons, the most abundant subtype of GABAergic interneurons in the RSC,[22] in contextual fear memory are yet to be elucidated. As RSC is also one of the first brain regions affected by β-amyloid accumulation in early Alzheimer's disease (AD),[17–21] which has been suggested to be highly related to memory deficits in AD,[13,20,23] we first set out to compare the ensemble dynamics of RSC PV interneurons during contextual fear memory encoding and retrieval between control mice and 5XFAD mouse model of AD. To do so, we injected AAV-DIO-GCaMP6s into the granular RSC of the control PV-Cre mice and 5XFAD/PV-Cre mice that showed β-amyloid accumulations (Figure 1A), from which longitudinal Ca^{2+} imaging of GCaMP6s-expressing PV interneurons was performed using a miniaturized microscope during a contextual fear memory task (Figure 1B). In the task, mice were first habituated to the test chamber (day 1, habituation). A day later (day 2), mice were placed in the same chamber for contextual fear conditioning, during which associative memory between the context of the chamber and the 1-s-long aversive electric foot shocks was formed.[24] On the third day (day 3), mice were returned to the chamber for the testing of contextual fear memory retrieval, measured as freezing behavior (Figures 1B and 1C). In 5XFAD/PV-Cre mice, freezing behavior was significantly decreased during contextual fear memory retrieval sessions compared with PV-Cre mice (Figure 1C), confirming that contextual fear memory retrieval is impaired in 5XFAD/PV-Cre mice. Such deficits in contextual fear memory retrieval in 5XFAD/PV-Cre mice were similar to those observed in 5XFAD mice (Figure 1C), indicating that the differences in background strains in the mouse model of AD had negligible effect on

Please cite this article in press as: Park et al., Memory encoding and retrieval by retrosplenial parvalbumin interneurons are impaired in Alzheimer's disease model mice, Current Biology (2023), https://doi.org/10.1016/j.cub.2023.12.014

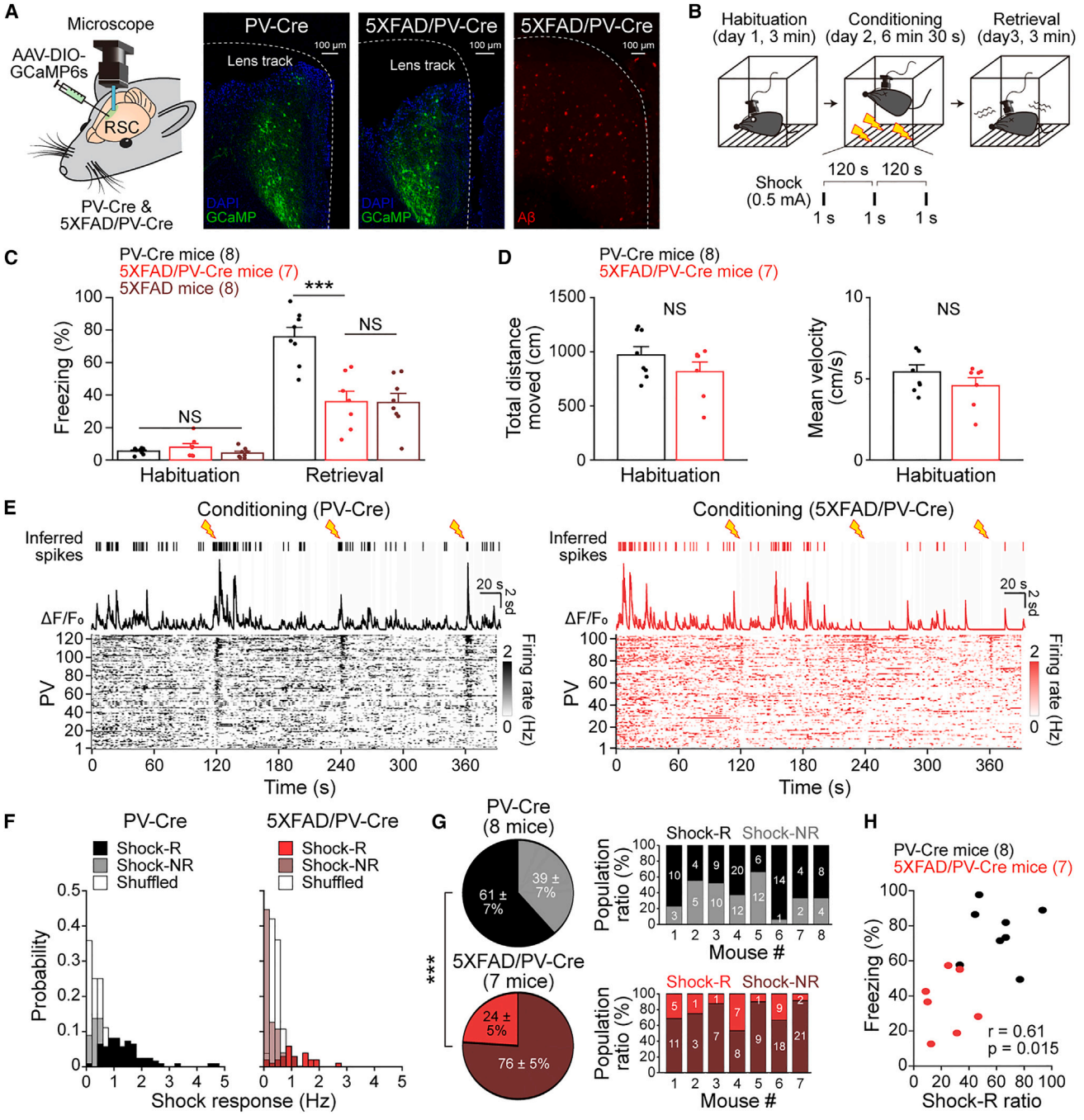

Figure 1. Encoding of contextual fear memory by PV interneurons in the granular retrosplenial cortex is impaired in 5XFAD/PV-Cre mice

(A) Experimental design for Ca^{2+} imaging from mice using a miniaturized microscope during contextual fear memory task. AAV-DIO-GCaMP6s virus was injected in the granular retrosplenial cortex (RSC) of PV-Cre and 5XFAD/PV-Cre mice, followed by a gradient-index (GRIN) lens implant (first column). Fluorescent images (second and third column) of virally expressed GCaMP6s in the granular RSC PV interneurons and β-amyloid (Aβ) in the granular RSC of 5XFAD/PV-Cre mouse (fourth column).

(B) Schematic illustration of contextual fear memory task consisting of habituation, contextual fear conditioning (conditioning), and contextual fear memory retrieval (retrieval) sessions.

(C) Averaged freezing behavior percentage of PV-Cre mice, 5XFAD/PV-Cre mice, and 5XFAD mice during habituation and retrieval sessions of contextual fear memory task (one-way ANOVA with post hoc Tukey's test, habituation, $F(2, 20) = 1.53$, $p = 0.24$; retrieval, $F(2, 20) = 15.80$, $p < 0.001$).

(D) Averaged total distance travelled (left) and mean velocity (right) of PV-Cre mice and 5XFAD/PV-Cre mice during habituation session (unpaired Student's t test, total distance traveled, $t(13) = 1.32$, $p = 0.21$; mean velocity, $t(13) = 1.30$, $p = 0.21$).

(E) Representative raw Ca^{2+} signals ($\triangle F/F_0$) of a single PV interneuron in RSC of PV-Cre mouse (black) or 5XFAD/PV-Cre mouse (red) from which deconvoluted spikes were extracted during conditioning session (inferred spikes). RSC neuronal firing rate map of total imaged PV interneurons during conditioning session.

(legend continued on next page)

Please cite this article in press as: Park et al., Memory encoding and retrieval by retrosplenial parvalbumin interneurons are impaired in Alzheimer's disease model mice, Current Biology (2023), https://doi.org/10.1016/j.cub.2023.12.014

memory deficits in 5XFAD/PV-Cre mice (see STAR Methods) and were independent of locomotion of 5XFAD/PV-Cre mice (Figure 1D). From the Ca^{2+} signals of neural ensembles acquired during the entire contextual fear memory task, we first analyzed how memory encoding is represented in the Ca^{2+} dynamics of PV interneuron ensembles. Extraction of spikes by deconvolutions of Ca^{2+} signals (Figure 1E) during a contextual fear conditioning session revealed that subpopulations of PV interneuron ensembles were responsive to aversive electric foot shocks, herein termed shock-responsive (shock-R) neurons, while the rest were not responsive to aversive electric foot shocks, herein termed shock non-responsive (shock-NR) neurons (Figures 1E–1G). A PV interneuron was defined to be shock-R if the spike firing rate in response to the electric foot shocks (shock response) exceeded the 95th percentile of the probability distribution of randomly shuffled shock response of the given neuron, while the remaining neurons were defined as shock-NR neurons (Figure 1F). Based on these analyses, in PV-Cre mice, 61% ± 7% of PV interneurons were shock-R while 39% ± 7% of PV interneurons were shock-NR (8 mice; Figure 1G). However, in 5XFAD/PV-Cre mice, only 24% ± 5% of PV interneurons were shock-R, while 76% ± 5% of PV interneurons were shock-NR (7 mice; Figure 1G). Overall, the population of shock-R PV interneurons that responded to contextual fear conditioning in each mouse was significantly lower in 5XFAD/PV-Cre mice compared with PV-Cre mice (Figure 1G). Such differences were not due to differences in PV interneurons' baseline activity between PV-Cre and 5XFAD/PV-Cre mice (Figure S1). The lower shock-R ratio in the 5XFAD/PV-Cre mice correlated with the low freezing ratio during the contextual fear memory retrieval session (Figure 1H). These results could also be captured by analyses repeated with Ca^{2+} transients (Figure S2), indicating that encoding of contextual fear memory by RSC PV interneurons is impaired in 5XFAD/PV-Cre mice.

Selective upregulation of memory-encoding PV interneuron ensemble dynamics during memory retrieval is disrupted in 5XFAD/PV-Cre mice

We next investigated how the recruitment of contextual fear memory-encoding shock-R PV interneurons shapes the inhibitory ensemble dynamics underlying contextual fear memory retrieval in control PV-Cre mice and, consequently, how the decrease in shock-R PV interneurons in 5XFAD/PV-Cre mice affects inhibitory ensemble dynamics underlying memory retrieval. Analysis of PV interneuron ensemble activities during contextual fear memory retrieval session in PV-Cre mice (Figure 2A) revealed that only shock-R PV interneurons, but not shock-NR PV interneurons, selectively increased their spike firing rates compared with the habituation session (Figure 2B). In contrast, in 5XFAD/PV-Cre mice, no changes were observed in spike firing rates during contextual fear memory retrieval and habituation sessions in either shock-R or shock-NR PV interneurons (Figures 2A and 2B). Thus, the selective increase in shock-R PV interneuron ensemble activities during contextual fear memory retrieval observed in PV-Cre mice was completely absent in 5XFAD/PV-Cre mice. Such changes in ensemble activities were independent of locomotion per se, as the correlations between neural activities and mouse velocity in both PV-Cre and 5XFAD/PV-Cre were low (Figure 2C).

As freezing behavior is considered to be the behavioral correlate of contextual fear memory retrieval, we further investigated how ensemble activities of PV interneurons are related to freezing and unfreezing epochs during the memory retrieval session. The firing rates of shock-R PV interneurons selectively increased during the freezing epoch in PV-Cre mice compared with the unfreezing epoch (Figure 2D, black), while in 5XFAD/PV-Cre mice, shock-R PV interneurons' spike firing rates were not different in freezing and non-freezing epochs (Figure 2D, red). To further characterize the ensemble dynamics of shock-R PV interneurons during the freezing and unfreezing epochs, *Z* scored neuronal activities were analyzed. We found that the majority of shock-R PV interneurons in PV-Cre mice showed upregulated *Z* scored neuronal activities during the freezing epochs (58% ± 6%; Figures 2E–2G), while subpopulations of shock-R PV interneurons showed either no changes (35% ± 7%; Figure 2G) or suppressed *Z* scored neuronal activities (7% ± 4%; Figure 2G). Subpopulations of shock-R PV interneurons that were upregulated during the freezing epoch of contextual fear memory retrieval were selectively suppressed in *Z* scores during the unfreezing epoch, showing bi-directional modulation of ensemble activities depending on the behavioral states (Figure S3). In contrast, the majority of shock-R PV interneurons in 5XFAD/PV-Cre mice showed no changes in *Z* scored neuronal activities, consequently showing significantly different ensemble dynamics during both the freezing (92% ± 6%; Figures 2E–2G) and unfreezing epochs (87% ± 7%; Figure S3) compared with shock-R PV interneurons in PV-Cre mice. Also, analysis of shock-NR PV interneurons showed no differences in spike firing rates (Figure 2H) nor *Z* scored neural activities during freezing and unfreezing epochs of retrieval sessions in PV-Cre mice and in 5XFAD/PV-Cre mice (Figures 2I–2K and S3). Similar results were obtained when analyses were repeated using Ca^{2+} transients (Figure S4). Together, these results suggest that selective upregulation of shock-R PV interneuron ensemble dynamics during the freezing epoch plays a key role in contextual fear memory retrieval in PV-Cre control mice, while disruption of shock-R PV interneuron ensemble dynamics in 5XFAD/PV-Cre mice may explain deficits in their contextual fear memory retrieval.

(F) Probability distributions of spike firing rate of shock-responsive (shock-R) and shock non-responsive (shock-NR) PV interneurons from PV-Cre mice or 5XFAD/PV-Cre mice in response to electric foot shocks (shock response) plotted together with the randomly shuffled shock responses for comparison (white).
(G) Pie chart (left) showing population ratio of shock-R and shock-NR PV interneurons in PV-Cre and 5XFAD/PV-Cre mice (unpaired Student's t test, PV-Cre vs. 5XFAD/PV-Cre, upregulated, shock-R, $t(13) = 4.23$, $p < 0.001$; shock-NR, $t(13) = -4.23$, $p < 0.001$). Bar graph (right) showing population ratio of shock-R and shock-NR PV interneurons in each individual PV-Cre and 5XFAD/PV-Cre mouse.
(H) Shock-R PV interneuron ratio versus averaged freezing behavior percentage of PV-Cre mice and 5XFAD/PV-Cre mice. r indicates correlation coefficient between Shock-R PV interneuron ratio and averaged freezing behavior percentage. p indicates p value for testing the hypothesis of no correlation. Data are represented as mean ± SEM. ***$p < 0.001$, NS: $p > 0.05$ for one-way ANOVA with post hoc Tukey's test (C) and unpaired Student's t test (D and G).
See also Figures S1 and S2.

Please cite this article in press as: Park et al., Memory encoding and retrieval by retrosplenial parvalbumin interneurons are impaired in Alzheimer's disease model mice, Current Biology (2023), https://doi.org/10.1016/j.cub.2023.12.014

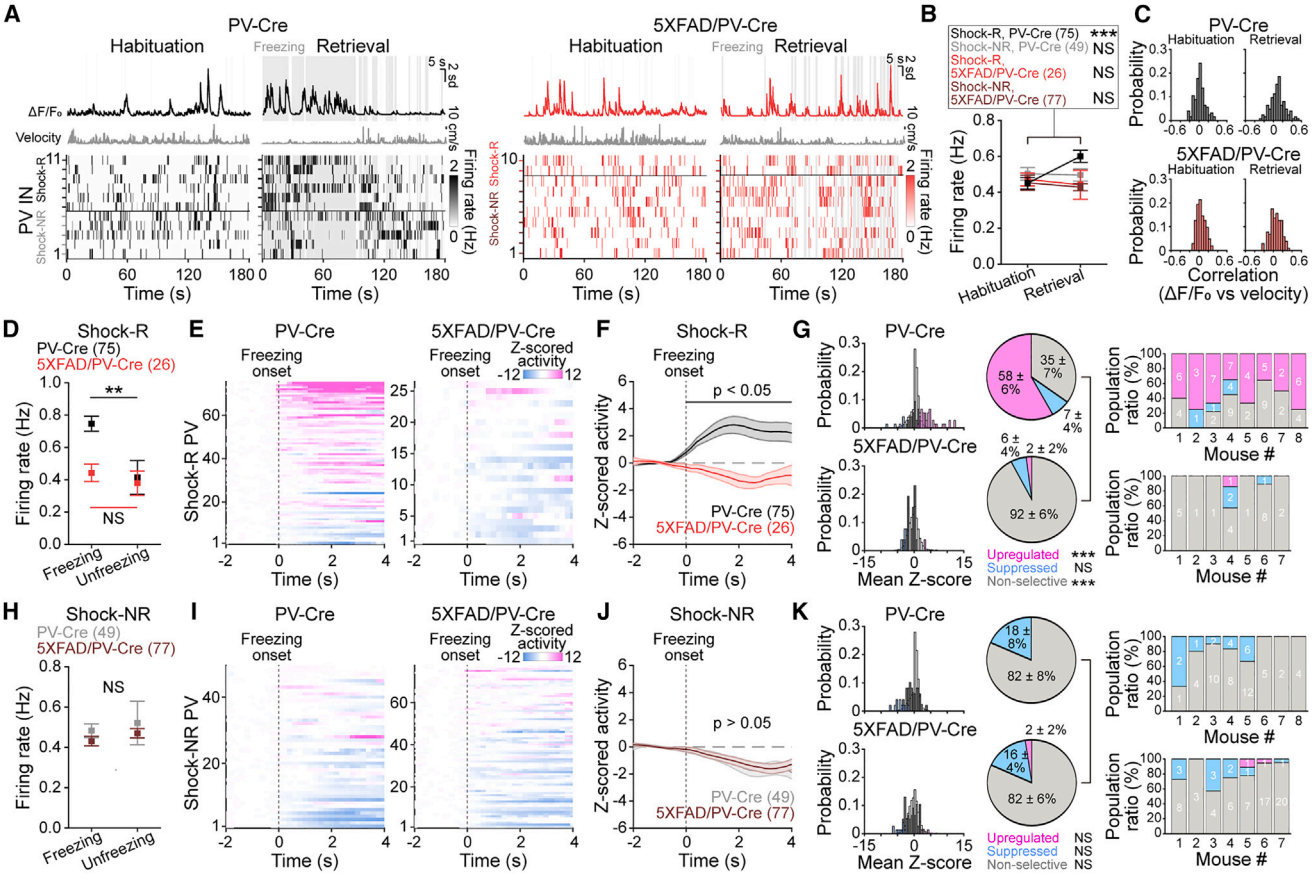

Figure 2. Selective upregulation of contextual fear memory-encoding PV interneuron ensemble dynamics in the granular retrosplenial cortex during memory retrieval is disrupted in 5XFAD/PV-Cre mice

(A) Representative raw Ca^{2+} signals ($\triangle F/F_0$) of a single PV interneuron in the granular retrosplenial cortex (RSC) of PV-Cre mouse (black, top) or 5XFAD/PV-Cre mouse (red, top) during habituation and retrieval sessions. Corresponding velocity of PV-Cre or 5XFAD/PV-Cre mice (gray, middle). RSC neuronal firing rate map (bottom) of representative PV interneurons from the same mouse for each session.

(B) Averaged firing rate of shock responsive (shock-R) and shock non-responsive (shock-NR) PV interneurons for each session (paired Student's t test, PV-Cre, shock-R, $t(74) = -3.78$, $p < 0.001$; shock-NR, $t(48) = 0.16$, $p = 0.87$; 5XFAD/PV-Cre, shock-R, $t(25) = 0.41$, $p = 0.69$; shock-NR, $t(76) = 0.61$, $p = 0.54$).

(C) Probability distributions of correlation coefficient between Ca^{2+} signals from all imaged PV interneurons and the velocity of corresponding PV-Cre mice (top) or 5XFAD/PV-Cre mice (bottom) during habituation and retrieval sessions.

(D) Averaged firing rate of shock-R PV interneurons during freezing and unfreezing epochs of retrieval session (paired Student's t test, PV-Cre, $t(74) = 3.00$, $p = 0.004$; 5XFAD/PV-Cre, $t(25) = 1.01$, $p = 0.32$).

(E) *Z* scored neuronal activity map of shock-R PV interneurons at the onset of freezing epoch in PV-Cre mice (left) and 5XFAD/PV-Cre mice (right).

(F) Averaged *Z* cored neuronal activities of shock-R PV interneurons at the onset of freezing epoch. Solid line: mean *Z* scored activity in PV-Cre mice (black) and 5XFAD/PV-Cre mice (red). Shade: SEM. Black horizontal line: significant differences according to the permutation test.

(G) Probability distributions (left) of mean *Z* score of neuronal activities of shock-R PV interneurons during freezing epoch plotted together with the randomly shuffled mean *Z* score for comparison (white). Pie chart (middle) showing population ratio of upregulated, suppressed, and non-selective shock-R PV interneurons according to the mean *Z* score at the onset of the freezing epoch (unpaired Student's t test, PV-Cre vs. 5XFAD/PV-Cre, upregulated, $t(13) = 8.73$, $p < 0.001$; suppressed, $t(13) = 0.24$, $p = 0.81$; non-selective, $t(13) = -6.13$, $p < 0.001$). Bar graph (right) showing population ratio of upregulated, suppressed, and non-selective shock-R PV interneurons in each individual PV-Cre and 5XFAD/PV-Cre mouse.

(H–K) Same with (D)–(G), but for shock-NR interneurons from PV-Cre mice or 5XFAD/PV-Cre mice (G, paired Student's t test, PV-Cre: $t(48) = -0.35$, $p = 0.73$; 5XFAD/PV-Cre: $t(76) = -1.30$, $p = 0.20$), (J, unpaired Student's t test, upregulated, $t(13) = -1.55$, $p = 0.15$; suppressed, $t(13) = 0.24$, $p = 0.82$; non-selective, $t(13) = -0.01$, $p = 0.99$). Data are represented as mean ± SEM. ***$p < 0.001$, **$p < 0.01$, NS.: $p > 0.05$ for paired (B, D, and H) and unpaired Student's t test (G and K). Permutation test (F and J).

See also Figures S3 and S4.

Contextual fear memory-induced potentiation of PV interneuron-mediated inhibition is impaired in 5XFAD/PV-Cre mice

Thus far, we found that contextual fear memory-encoding shock-R PV interneuron ensemble activities were selectively and dynamically upregulated during memory retrieval session in the control PV-Cre mice. Thus, the synaptic strengthening of PV interneuron-mediated inhibition in the network could serve as one possible circuit mechanism underlying the changes in contextual fear conditioning-induced RSC PV interneuron ensemble dynamics. To directly test this hypothesis, we performed *in vitro* whole-cell voltage-clamp recordings to measure

Please cite this article in press as: Park et al., Memory encoding and retrieval by retrosplenial parvalbumin interneurons are impaired in Alzheimer's disease model mice, Current Biology (2023), https://doi.org/10.1016/j.cub.2023.12.014

CellPress
OPEN ACCESS

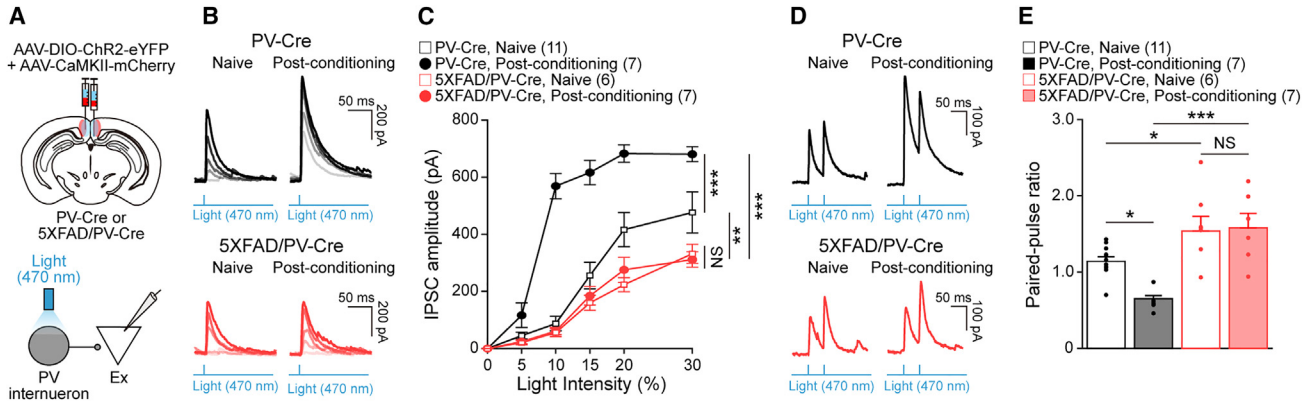

Figure 3. Contextual fear conditioning-induced potentiation of PV interneuron-mediated inhibition in the granular retrosplenial cortex is impaired in 5XFAD/PV-Cre mice

(A) Experimental design (top) for simultaneous virus injection of AAV-DIO-ChR2-eYFP and AAV-CaMKII-mCherry in the granular retrosplenial cortex (RSC). Schematic showing *in vitro* whole-cell voltage-clamp recordings from excitatory neurons (Ex) during blue light (470 nm) stimulation of ChR2-expressing PV interneurons in RSC.

(B and C) Representative PV interneuron-evoked inhibitory postsynaptic currents (IPSCs) in response to different light stimulation intensities (B) and stimulus-response curve (C), recorded from RSC Ex of PV-Cre (top) and 5XFAD/PV-Cre mice (bottom) without (Naive) or after contextual fear conditioning (post-conditioning) (three-way ANOVA with post hoc Tukey's test, three-way interaction, $F(5, 162) = 4.90$, $p < 0.001$).

(D and E) Representative PV interneuron-evoked IPSCs in response to light stimulations (2 pulses, 20 Hz) (D) and paired-pulse ratio of the 2nd IPSC/1st IPSC (E), recorded from RSC Ex for each condition (two-way ANOVA with post hoc Tukey's test, two-way interaction, $F(1, 27) = 4.44$, $p = 0.04$). Data are represented as mean ± SEM. ***$p < 0.001$, **$p < 0.01$, *$p < 0.05$, NS.: $p > 0.05$ for three-way (C) and two-way ANOVA with post hoc Tukey's test (E).

the changes in PV interneuron-mediated inhibition following contextual fear conditioning. Mice were injected with AAV-ChR2-DIO-eYFP (channelrhodopsin-2 [ChR2]) and AAV-CaMKII-mCherry in the granular RSC (Figure 3A, top), and from brain slices cut from either naive mice (Naive) that did not receive any electric foot shocks during the conditioning session or from mice that underwent contextual fear conditioning (post-conditioning), PV interneuron-evoked inhibitory postsynaptic currents (PV-eIPSCs) were recorded from mCherry-expressing excitatory neurons *in vitro* by stimulating ChR2-expressing PV interneurons using blue light (470 nm; Figure 3A, bottom). In response to incrementing intensities of single-pulse blue light stimulation, PV-eIPSCs in the stimulus-response (S-R) curve revealed that PV-eIPSCs amplitudes in the naive 5XFAD/PV-Cre mice were significantly decreased compared with those in the naive PV-Cre mice, indicating the reduction of responsiveness in PV interneurons in 5XFAD/PV-Cre mice, even in naive condition (Figures 3B and 3C). PV-eIPSCs amplitudes were significantly increased in brain slices cut from PV-Cre mice post-conditioning compared with those from the naive PV-Cre mice (Figure 3C, black), but such changes were absent in 5XFAD/PV-Cre mice (Figure 3C, red). These results indicate that not only PV interneurons' responsiveness is impaired in 5XFAD/PV-Cre mice in the naive condition but that the potentiation of PV interneuron-mediated inhibition at the PV-to-excitatory neuron synapse post-conditioning is also impaired. To further investigate the short-term synaptic changes of PV interneuron-mediated inhibition, paired-pulse ratio (PPR) was measured by delivering two pulses of blue light stimulation at 20 Hz to ChR2-expressing PV interneurons (Figures 3D and 3E), where stimulation frequency (20 Hz) was selected to reflect PV interneurons' spike frequencies during baseline activity (Figure S1). Paired-pulse facilitation of PV-eIPSCs in the naive PV-Cre mice was converted to paired-pulse depression in PV-Cre mice post-conditioning (Figures 3D and 3E, black), indicating that contextual fear conditioning induced presynaptic strengthening of PV-eIPSCs to excitatory neurons. However, paired-pulse facilitation in the naive 5XFAD/PV-Cre mice was unaltered in 5XFAD/PV-Cre mice, even post-conditioning (Figures 3D and 3E, red). Based on the S-R curve and PPR analyses, it can be inferred that contextual fear conditioning-induced enhancement of PV interneuron responsiveness and synaptic strengthening of PV interneuron-mediated inhibition may have contributed to the upregulation of PV interneurons' ensemble dynamics during the freezing epoch of contextual fear memory retrieval. In contrast, the reduced responsiveness and synaptic dysfunctions of PV interneurons may have disrupted the recruitment of shock-R PV interneurons during contextual fear memory encoding, leading to the failure in shaping the ensemble dynamics underlying contextual fear memory retrieval in 5XFAD/PV-Cre mice.

Optogenetic activation of PV interneurons during contextual fear memory encoding restores memory retrieval in 5XFAD/PV-Cre mice

Thus far, we found that failure of PV interneurons in 5XFAD/PV-Cre mice to encode contextual fear memory led to the disruption of ensemble dynamics required for memory retrieval. Thus, we next tested whether disruption of the recruitment of contextual fear memory encoding in PV interneurons in PV-Cre mice could mimic the memory retrieval deficits observed in 5XFAD/PV-Cre mice. We injected AAV-DIO-NpHR3.0-eYFP bilaterally into the granular RSC to optogenetically silence NpHR3.0-expressing PV interneurons using yellow light (595 nm) delivered through optic fibers (Figure 4A, top) when electric foot shocks were delivered during contextual fear conditioning (Figure 4B). In these mice, the freezing ratio during memory retrieval sessions

Please cite this article in press as: Park et al., Memory encoding and retrieval by retrosplenial parvalbumin interneurons are impaired in Alzheimer's disease model mice, Current Biology (2023), https://doi.org/10.1016/j.cub.2023.12.014

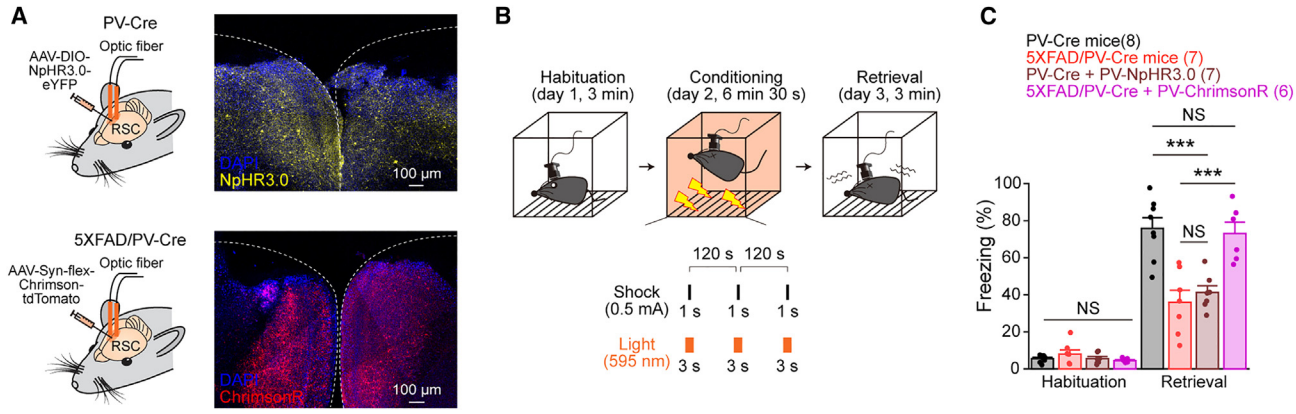

Figure 4. Optogenetic activation of contextual fear memory-encoding PV interneurons in the granular retrosplenial cortex restores memory retrieval in 5XFAD/PV-Cre mice

(A) Experimental design for optogenetic inactivation (top, left) or activation (bottom, left) of PV interneurons in the granular retrosplenial cortex (RSC) during contextual fear conditioning. AAV-DIO-NpHR3.0-eYFP (top) or AAV-Syn-flex-ChrimsonR-tdTomato (bottom) was injected bilaterally into the granular RSC of PV-Cre mice or 5XFAD/PV-Cre mice, respectively, followed by optic fiber implant. Fluorescent images of virally expressed NpHR3.0 (top, right) or ChrimsonR (bottom, right) on the granular RSC PV interneurons.

(B) Schematic illustration of contextual fear memory task with optogenetic inactivation or activation of RSC PV interneurons during contextual fear conditioning.

(C) Averaged freezing behavior percentage of each condition during habituation and retrieval sessions of contextual fear memory task (one-way ANOVA with post hoc Tukey's test, habituation, $F(3, 24) = 1.11$, $p = 0.37$; retrieval, $F(3, 24) = 14.00$, $p < 0.001$). Data are represented as mean ± SEM. ***$p < 0.001$, NS: $p > 0.05$ for one-way ANOVA with post hoc Tukey's test (C).

significantly decreased compared with that in PV-Cre mice, which was similar to the freezing ratio observed in 5XFAD/PV-Cre mice (Figure 4C). These results indicate that the silencing of PV interneurons to disrupt the recruitment of shock-R PV interneurons during contextual fear memory encoding could mimic the deficits in memory retrieval observed in 5XFAD/PV-Cre mice. If disruption of the recruitment of contextual fear memory encoding by PV interneurons can explain deficits in memory retrieval, increased recruitment of PV interneurons during contextual fear memory encoding in 5XFAD/PV-Cre mice could restore memory retrieval. To test this hypothesis in 5XFAD/PV-Cre mice, we injected AAV-Syn-Flex-ChrimsonR-tdTomato bilaterally into the granular RSC and activated ChrimsonR-expressing PV interneurons using yellow light (595 nm) through optic fibers (Figure 4A, bottom) when electric foot shocks were delivered during contextual fear conditioning (Figure 4B). Interestingly, yellow light stimulation of ChrimsonR-expressing PV interneurons increased the freezing ratio during retrieval sessions in 5XFAD/PV-Cre mice to a similar level as that in PV-Cre mice (Figure 4C). Overall, our optogenetic manipulation results revealed that the recruitment of contextual fear memory-encoding RSC PV interneurons during contextual fear conditioning can gate memory retrieval in the healthy brain, and optogenetic activation of dysfunctional RSC PV interneurons during memory encoding in 5XFAD/PV-Cre mice is sufficient to restore memory retrieval deficits.

DISCUSSION

By combining *in vivo* and *in vitro* neural circuit analysis, we found that RSC PV interneurons are involved in contextual fear memory encoding (Figure 1) and that memory-encoding PV interneuron ensemble dynamics were selectively upregulated during the memory retrieval session (Figure 2). Such memory-encoding PV interneuron ensemble dynamics could have been manifested by the potentiation of PV interneuron-mediated inhibition at the synaptic level after contextual fear conditioning (Figure 3). However, in 5XFAD/PV-Cre mice, disruption in the recruitment of contextual fear memory-encoding RSC PV interneurons consequently failed to shape the ensemble dynamics underlying memory retrieval in 5XFAD/PV-Cre mice (Figures 1 and 2), which could be associated with synaptic dysfunctions of PV interneurons (Figure 3). Optogenetic activation of PV interneurons in 5XFAD/PV-Cre during contextual fear conditioning to recruit more memory-encoding PV interneurons could fully restore deficits in memory retrieval in 5XFAD/PV-Cre mice, while optogenetic silencing of PV interneurons in the control PV-Cre mice to interfere with the recruitment of memory-encoding PV interneurons could mimic the deficits in memory retrieval in 5XFAD/PV-Cre mice (Figure 4). Together, these results suggest that the ensemble dynamics of contextual fear memory-encoding RSC PV interneurons represent memory retrieval while dysfunction of RSC PV interneurons disrupts the recruitment of memory-encoding PV interneurons and their ensemble dynamics underlying memory encoding and retrieval, leading to memory deficits in the 5XFAD mouse model of AD.

Our results demonstrate that RSC PV interneurons play important roles in encoding and retrieval of memory, which is in line with the many previous studies showing GABAergic interneurons' involvement in encoding memory.[8–12] Moreover, our results suggest that RSC PV interneurons also display properties of inhibitory memory engram[9] as (1) they were activated during memory encoding, (Figure 1), (2) memory-encoding RSC PV interneurons were selectively re-activated during memory retrieval (Figure 2), and (3) synaptic strengthening of PV interneuron-mediated inhibition after memory encoding was observed (Figure 3). Thus, it is possible that the inhibitory memory engrams identified here could perform many of the suggested functions

Please cite this article in press as: Park et al., Memory encoding and retrieval by retrosplenial parvalbumin interneurons are impaired in Alzheimer's disease model mice, Current Biology (2023), https://doi.org/10.1016/j.cub.2023.12.014

of inhibitory engrams, such as fine-tuning of excitatory engrams in RSC[14,15] by controlling their size,[11,25] suppressing the irrelevant excitatory neurons,[9] and activating the appropriate excitatory memory engrams through disinhibition.[8,10,12,26,27] As inhibitory engrams are suggested to be "a negative image" of excitatory engrams,[9] it can be predicted that the ensemble dynamics of RSC excitatory neurons will be downregulated during freezing epochs while upregulated during the unfreezing epoch of memory retrieval. In fact, subpopulations of RSC excitatory neurons are known to process spatial context information during an animal's navigating movement,[13] especially with the recent discovery of egocentric boundary vector/border cells and vertex cells in the RSC.[28–30] Thus, spatial context information processed by RSC excitatory neurons may be activated during the unfreezing epoch during memory retrieval, which in turn may activate shock-R PV interneurons to initiate freezing behavior. Also, as RSC is known to project to motor cortex,[31] PV interneurons may inhibit RSC projection to the motor cortex to initiate freezing activity, which will be interesting to explore in the future.

In our study, optogenetic activation of RSC PV interneurons during contextual fear conditioning to recruit more shock-R PV interneurons in 5XFAD/PV-Cre mice restored memory retrieval, further underscoring the critical roles of memory-encoding RSC PV interneurons for successful memory retrieval (Figure 4). Such a result may explain how the dysfunction of PV interneurons has been associated with the pathological features of AD[1–3,32–39] and how manipulations of PV interneurons in AD through optogenetic stimulation,[1,2,32,33] genetic manipulation,[35] and PV interneuron transplant[36] have ameliorated memory deficits in AD. In addition to the disruption of inhibitory ensemble dynamics, dysfunction of RSC PV interneurons may have led to excitation-inhibition (E-I) imbalance[4,5,40–42] and the hyperexcitability[34,35,43–45] of neural networks in AD, which have been reported to disrupt the neural correlates of memory, such as the network oscillations[1,2,32–35,42,46–51] and synaptic plasticity[2,41,52–56] in animal models of AD or in AD patients. Thus, elucidating how impairments of network oscillations and synaptic plasticity are associated with disruption of inhibitory engrams of PV interneurons may further expand our understanding on the dysfunctions of neural correlates of memory in AD.

Despite these results, there are many limitations in our study. Firstly, we used deconvolution methods (OASIS [online active set method to infer spikes])[57–60] in inferring putative spikes from PV interneurons. Because this deconvolution method has been developed using data from excitatory neurons,[57] and as PV interneurons have higher spike firing rates than excitatory neurons, care must be taken in directly applying the deconvolution methods to PV interneuron Ca^{2+} data, as it might lead to inaccurate spike inference for PV interneurons.[61] However, there are studies that have already used deconvoluted PV interneuron spikes from Ca^{2+} imaging data,[59,62–64] and PV interneuron Ca^{2+} transient event-based analyses of our results (Figures S2 and S4) were in fact consistent with results analyzed with deconvoluted spikes, supporting the validity of our results. Another limitation of our study is that we could not rule out the effect of electric foot shock-induced stress or pain on changes observed in RSC PV interneuron ensemble activities, which will require further behavioral dissection and validation in the future. Nevertheless, our results provide experimental evidence for how contextual fear memory encoding by RSC PV interneurons contributes to shaping the ensemble dynamics underling memory retrieval in the cortical network and how dysfunction of RSC PV interneurons disrupts the neural representation of memory encoding and retrieval, leading to memory deficits in AD. Our results provide insight into the neural circuit mechanisms of memory processing and point toward potential therapeutic targets in AD.

STAR★METHODS

Detailed methods are provided in the online version of this paper and include the following:

- KEY RESOURCES TABLE
- RESOURCE AVAILABILITY
  - Lead contact
  - Materials availability
  - Data and code availability
- EXPERIMENTAL MODEL AND SUBJECT DETAILS
  - Animals
- METHOD DETAILS
  - Virus and stereotaxic surgery for *in vivo* Ca^{2+} imaging
  - Virus and stereotaxic surgery for *in vitro* optogenetic experiments
  - Virus and stereotaxic surgery for *in vivo* optogenetic experiments
  - *In vivo* Ca^{2+} imaging and signal processing
  - Contextual fear memory task
  - Histology and immunohistochemistry
  - Neural selectivity analysis
  - *In vitro* RSC slice preparation
  - *In vitro* whole-cell patch-clamp recordings
- QUANTIFICATION AND STATISTICAL ANALYSIS
  - Statistics

SUPPLEMENTAL INFORMATION

Supplemental information can be found online at https://doi.org/10.1016/j.cub.2023.12.014.

ACKNOWLEDGMENTS

This research was supported by the Korea Health Technology R&D Project through the Korea Health Industry Development Institute (KHIDI) and the Korea Dementia Research Center (KDRC), which was funded by the Ministry of Health & Welfare and the Ministry of Science and ICT, Republic of Korea (grant no. HU20C0233). We thank Mr. Yoonsoo Yeo for help with animal behavior experiments.

AUTHOR CONTRIBUTIONS

K.P., M.M.K., and J.K. conceived the experiments. K.P. conducted the experiments and analyzed the data. K.P. and J.K. interpreted the results. J.K. wrote the original draft of the manuscript. K.P., M.M.K., and J.K. reviewed and edited the final manuscript. J.K. acquired funding and supervised the project.

DECLARATION OF INTERESTS

The authors declare no competing interests.

Received: July 7, 2023
Revised: October 23, 2023
Accepted: December 6, 2023
Published: December 28, 2023

REFERENCES

1. Chung, H., Park, K., Jang, H.J., Kohl, M.M., and Kwag, J. (2020). Dissociation of somatostatin and parvalbumin interneurons circuit dysfunctions underlying hippocampal theta and gamma oscillations impaired by amyloid beta oligomers in vivo. Brain Struct. Funct. *225*, 935–954. https://www.ncbi.nlm.nih.gov/pubmed/32107637.
2. Park, K., Lee, J., Jang, H.J., Richards, B.A., Kohl, M.M., and Kwag, J. (2020). Optogenetic activation of parvalbumin and somatostatin interneurons selectively restores theta-nested gamma oscillations and oscillation-induced spike timing-dependent long-term potentiation impaired by amyloid beta oligomers. BMC Biol. *18*, 7. https://www.ncbi.nlm.nih.gov/pubmed/31937327.
3. Xu, Y., Zhao, M., Han, Y., and Zhang, H. (2020). GABAergic inhibitory interneuron deficits in Alzheimer's disease: implications for treatment. Front. Neurosci. *14*, 660. https://www.ncbi.nlm.nih.gov/pubmed/32714136.
4. Petrache, A.L., Rajulawalla, A., Shi, A., Wetzel, A., Saito, T., Saido, T.C., Harvey, K., and Ali, A.B. (2019). Aberrant excitatory-inhibitory synaptic mechanisms in entorhinal cortex microcircuits during the pathogenesis of Alzheimer's disease. Cereb. Cortex *29*, 1834–1850. https://www.ncbi.nlm.nih.gov/pubmed/30766992.
5. Shi, A., Petrache, A.L., Shi, J., and Ali, A.B. (2020). Preserved calretinin interneurons in an app model of Alzheimer's disease disrupt hippocampal inhibition via upregulated P2Y1 purinoreceptors. Cereb. Cortex *30*, 1272–1290. https://www.ncbi.nlm.nih.gov/pubmed/31407772.
6. Palop, J.J., Chin, J., Roberson, E.D., Wang, J., Thwin, M.T., Bien-Ly, N., Yoo, J., Ho, K.O., Yu, G.Q., Kreitzer, A., et al. (2007). Aberrant excitatory neuronal activity and compensatory remodeling of inhibitory hippocampal circuits in mouse models of Alzheimer's disease. Neuron *55*, 697–711. https://www.ncbi.nlm.nih.gov/pubmed/17785178.
7. Alberdi, E., Sánchez-Gómez, M.V., Cavaliere, F., Pérez-Samartín, A., Zugaza, J.L., Trullas, R., Domercq, M., and Matute, C. (2010). Amyloid beta oligomers induce Ca2+ dysregulation and neuronal death through activation of ionotropic glutamate receptors. Cell Calcium *47*, 264–272. https://www.ncbi.nlm.nih.gov/pubmed/20061018.
8. Cummings, K.A., and Clem, R.L. (2020). Prefrontal somatostatin interneurons encode fear memory. Nat. Neurosci. *23*, 61–74. https://www.ncbi.nlm.nih.gov/pubmed/31844314.
9. Barron, H.C., Vogels, T.P., Behrens, T.E., and Ramaswami, M. (2017). Inhibitory engrams in perception and memory. Proc. Natl. Acad. Sci. USA *114*, 6666–6674. https://www.ncbi.nlm.nih.gov/pubmed/28611219.
10. Courtin, J., Karalis, N., Gonzalez-Campo, C., Wurtz, H., and Herry, C. (2014). Persistence of amygdala gamma oscillations during extinction learning predicts spontaneous fear recovery. Neurobiol. Learn. Mem. *113*, 82–89. https://www.ncbi.nlm.nih.gov/pubmed/24091205.
11. Lovett-Barron, M., Kaifosh, P., Kheirbek, M.A., Danielson, N., Zaremba, J.D., Reardon, T.R., Turi, G.F., Hen, R., Zemelman, B.V., and Losonczy, A. (2014). Dendritic inhibition in the hippocampus supports fear learning. Science *343*, 857–863. https://www.ncbi.nlm.nih.gov/pubmed/24558155.
12. Wolff, S.B., Gründemann, J., Tovote, P., Krabbe, S., Jacobson, G.A., Müller, C., Herry, C., Ehrlich, I., Friedrich, R.W., Letzkus, J.J., et al. (2014). Amygdala interneuron subtypes control fear learning through disinhibition. Nature *509*, 453–458. https://www.ncbi.nlm.nih.gov/pubmed/24814341.
13. Vann, S.D., Aggleton, J.P., and Maguire, E.A. (2009). What does the retrosplenial cortex do? Nat. Rev. Neurosci. *10*, 792–802. https://www.ncbi.nlm.nih.gov/pubmed/19812579.
14. de Sousa, A.F., Cowansage, K.K., Zutshi, I., Cardozo, L.M., Yoo, E.J., Leutgeb, S., and Mayford, M. (2019). Optogenetic reactivation of memory ensembles in the retrosplenial cortex induces systems consolidation. Proc. Natl. Acad. Sci. USA *116*, 8576–8581. https://www.ncbi.nlm.nih.gov/pubmed/30877252.
15. Cowansage, K.K., Shuman, T., Dillingham, B.C., Chang, A., Golshani, P., and Mayford, M. (2014). Direct reactivation of a coherent neocortical memory of context. Neuron *84*, 432–441. https://www.ncbi.nlm.nih.gov/pubmed/25308330.
16. Opalka, A.N., and Wang, D.V. (2020). Hippocampal efferents to retrosplenial cortex and lateral septum are required for memory acquisition. Learn. Mem. *27*, 310–318. https://www.ncbi.nlm.nih.gov/pubmed/32669386.
17. Talwar, P., Kushwaha, S., Chaturvedi, M., and Mahajan, V. (2021). Systematic review of different neuroimaging correlates in mild cognitive impairment and Alzheimer's disease. Clin. Neuroradiol. *31*, 953–967. https://www.ncbi.nlm.nih.gov/pubmed/34297137.
18. Poirier, G.L., Amin, E., Good, M.A., and Aggleton, J.P. (2011). Early-onset dysfunction of retrosplenial cortex precedes overt amyloid plaque formation in Tg2576 mice. Neuroscience *174*, 71–83. https://www.ncbi.nlm.nih.gov/pubmed/21093545.
19. Minoshima, S., Giordani, B., Berent, S., Frey, K.A., Foster, N.L., and Kuhl, D.E. (1997). Metabolic reduction in the posterior cingulate cortex in very early Alzheimer's disease. Ann. Neurol. *42*, 85–94. https://www.ncbi.nlm.nih.gov/pubmed/9225689.
20. Villain, N., Desgranges, B., Viader, F., de la Sayette, V., Mézenge, F., Landeau, B., Baron, J.C., Eustache, F., and Chételat, G. (2008). Relationships between hippocampal atrophy, white matter disruption, and gray matter hypometabolism in Alzheimer's disease. J. Neurosci. *28*, 6174–6181. https://www.ncbi.nlm.nih.gov/pubmed/18550759.
21. Kim, D.H., Kim, H.A., Han, Y.S., Jeon, W.K., and Han, J.S. (2020). Recognition memory impairments and amyloid-beta deposition of the retrosplenial cortex at the early stage of 5XFAD mice. Physiol. Behav. *222*, 112891. https://www.ncbi.nlm.nih.gov/pubmed/32442584.
22. Whissell, P.D., Cajanding, J.D., Fogel, N., and Kim, J.C. (2015). Comparative density of CCK- and PV-GABA cells within the cortex and hippocampus. Front. Neuroanat. *9*, 124. https://www.ncbi.nlm.nih.gov/pubmed/26441554.
23. Walsh, C., Ridler, T., Margetts-Smith, G., Garcia Garrido, M., Witton, J., Randall, A.D., and Brown, J.T. (2022). beta bursting in the retrosplenial cortex is a neurophysiological correlate of environmental novelty which is disrupted in a mouse model of Alzheimer's disease. J. Neurosci. *42*, 7094–7109. https://www.ncbi.nlm.nih.gov/pubmed/35927034.
24. Kim, J.J., and Fanselow, M.S. (1992). Modality-specific retrograde amnesia of fear. Science *256*, 675–677. https://www.ncbi.nlm.nih.gov/pubmed/1585183.
25. Stefanelli, T., Bertollini, C., Lüscher, C., Muller, D., and Mendez, P. (2016). Hippocampal somatostatin interneurons control the size of neuronal memory ensembles. Neuron *89*, 1074–1085. https://www.ncbi.nlm.nih.gov/pubmed/26875623.
26. Xu, H., Liu, L., Tian, Y., Wang, J., Li, J., Zheng, J., Zhao, H., He, M., Xu, T.L., Duan, S., et al. (2019). A disinhibitory microcircuit mediates conditioned social fear in the prefrontal cortex. Neuron *102*, 668–682.e5. https://www.ncbi.nlm.nih.gov/pubmed/30898376.
27. Letzkus, J.J., Wolff, S.B., and Lüthi, A. (2015). Disinhibition, a circuit mechanism for associative learning and memory. Neuron *88*, 264–276. https://www.ncbi.nlm.nih.gov/pubmed/26494276.
28. Alexander, A.S., Carstensen, L.C., Hinman, J.R., Raudies, F., Chapman, G.W., and Hasselmo, M.E. (2020). Egocentric boundary vector tuning of the retrosplenial cortex. Sci. Adv. *6*, eaaz2322. https://www.ncbi.nlm.nih.gov/pubmed/32128423.
29. van Wijngaarden, J.B., Babl, S.S., and Ito, H.T. (2020). Entorhinal-retrosplenial circuits for allocentric-egocentric transformation of boundary coding. eLife *9*, e59816. https://www.ncbi.nlm.nih.gov/pubmed/33138915.
30. Park, K., Yeo, Y., Shin, K., and Kwag, J. (2023). Egocentric vector coding of geometric vertex in the retrosplenial cortex. Preprint at bioRxiv. https://www.biorxiv.org/content/biorxiv/early/2023/09/05/2023.09.03.556136.full.pdf.

31. Franco, L.M., and Goard, M.J. (2021). A distributed circuit for associating environmental context with motor choice in retrosplenial cortex. Sci. Adv. *7*, eabf9815. https://www.ncbi.nlm.nih.gov/pubmed/34433557.

32. Etter, G., van der Veldt, S., Manseau, F., Zarrinkoub, I., Trillaud-Doppia, E., and Williams, S. (2019). Optogenetic gamma stimulation rescues memory impairments in an Alzheimer's disease mouse model. Nat. Commun. *10*, 5322. https://www.ncbi.nlm.nih.gov/pubmed/31757962.

33. Iaccarino, H.F., Singer, A.C., Martorell, A.J., Rudenko, A., Gao, F., Gillingham, T.Z., Mathys, H., Seo, J., Kritskiy, O., Abdurrob, F., et al. (2016). Gamma frequency entrainment attenuates amyloid load and modifies microglia. Nature *540*, 230–235. https://www.ncbi.nlm.nih.gov/pubmed/27929004.

34. Palop, J.J., and Mucke, L. (2016). Network abnormalities and interneuron dysfunction in Alzheimer disease. Nat. Rev. Neurosci. *17*, 777–792. https://www.ncbi.nlm.nih.gov/pubmed/27829687.

35. Verret, L., Mann, E.O., Hang, G.B., Barth, A.M., Cobos, I., Ho, K., Devidze, N., Masliah, E., Kreitzer, A.C., Mody, I., et al. (2012). Inhibitory interneuron deficit links altered network activity and cognitive dysfunction in Alzheimer model. Cell *149*, 708–721. https://www.ncbi.nlm.nih.gov/pubmed/22541439.

36. Martinez-Losa, M., Tracy, T.E., Ma, K., Verret, L., Clemente-Perez, A., Khan, A.S., Cobos, I., Ho, K., Gan, L., Mucke, L., et al. (2018). Nav1.1-overexpressing interneuron transplants restore brain rhythms and cognition in a mouse model of Alzheimer's disease. Neuron *98*, 75–89.e5. https://www.ncbi.nlm.nih.gov/pubmed/29551491.

37. Hijazi, S., Heistek, T.S., Scheltens, P., Neumann, U., Shimshek, D.R., Mansvelder, H.D., Smit, A.B., and van Kesteren, R.E. (2020). Early restoration of parvalbumin interneuron activity prevents memory loss and network hyperexcitability in a mouse model of Alzheimer's disease. Mol. Psychiatry *25*, 3380–3398. https://www.ncbi.nlm.nih.gov/pubmed/31431685.

38. Hijazi, S., Heistek, T.S., van der Loo, R., Mansvelder, H.D., Smit, A.B., and van Kesteren, R.E. (2020). Hyperexcitable parvalbumin interneurons render hippocampal circuitry vulnerable to amyloid beta. iScience *23*, 101271. https://www.ncbi.nlm.nih.gov/pubmed/32593000.

39. Hijazi, S., Smit, A.B., and van Kesteren, R.E. (2023). Fast-spiking parvalbumin-positive interneurons in brain physiology and Alzheimer's disease. Mol. Psychiatry. https://www.ncbi.nlm.nih.gov/pubmed/37419975.

40. Sun, B., Halabisky, B., Zhou, Y., Palop, J.J., Yu, G., Mucke, L., and Gan, L. (2009). Imbalance between GABAergic and glutamatergic transmission impairs adult neurogenesis in an animal model of Alzheimer's disease. Cell Stem Cell *5*, 624–633. https://www.ncbi.nlm.nih.gov/pubmed/19951690.

41. Lei, M., Xu, H., Li, Z., Wang, Z., O'Malley, T.T., Zhang, D., Walsh, D.M., Xu, P., Selkoe, D.J., and Li, S. (2016). Soluble Abeta oligomers impair hippocampal LTP by disrupting glutamatergic/GABAergic balance. Neurobiol. Dis. *85*, 111–121. https://www.ncbi.nlm.nih.gov/pubmed/26525100.

42. Kurudenkandy, F.R., Zilberter, M., Biverstål, H., Presto, J., Honcharenko, D., Strömberg, R., Johansson, J., Winblad, B., and Fisahn, A. (2014). Amyloid-beta-induced action potential desynchronization and degradation of hippocampal gamma oscillations is prevented by interference with peptide conformation change and aggregation. J. Neurosci. *34*, 11416–11425. https://www.ncbi.nlm.nih.gov/pubmed/25143621.

43. Busche, M.A., Eichhoff, G., Adelsberger, H., Abramowski, D., Wiederhold, K.H., Haass, C., Staufenbiel, M., Konnerth, A., and Garaschuk, O. (2008). Clusters of hyperactive neurons near amyloid plaques in a mouse model of Alzheimer's disease. Science *321*, 1686–1689. https://www.ncbi.nlm.nih.gov/pubmed/18802001.

44. Palop, J.J., and Mucke, L. (2010). Amyloid-beta-induced neuronal dysfunction in Alzheimer's disease: from synapses toward neural networks. Nat. Neurosci. *13*, 812–818. https://www.ncbi.nlm.nih.gov/pubmed/20581818.

45. Lerdkrai, C., Asavapanumas, N., Brawek, B., Kovalchuk, Y., Mojtahedi, N., Olmedillas Del Moral, M., and Garaschuk, O. (2018). Intracellular Ca^{2+} stores control in vivo neuronal hyperactivity in a mouse model of Alzheimer's disease. Proc. Natl. Acad. Sci. USA *115*, E1279–E1288. https://www.ncbi.nlm.nih.gov/pubmed/29358403.

46. Mably, A.J., and Colgin, L.L. (2018). Gamma oscillations in cognitive disorders. Curr. Opin. Neurobiol. *52*, 182–187. https://www.ncbi.nlm.nih.gov/pubmed/30121451.

47. van Deursen, J.A., Vuurman, E.F., Verhey, F.R., van Kranen-Mastenbroek, V.H., and Riedel, W.J. (2008). Increased EEG gamma band activity in Alzheimer's disease and mild cognitive impairment. J. Neural Transm. (Vienna) *115*, 1301–1311. https://www.ncbi.nlm.nih.gov/pubmed/18607528.

48. Goutagny, R., Gu, N., Cavanagh, C., Jackson, J., Chabot, J.G., Quirion, R., Krantic, S., and Williams, S. (2013). Alterations in hippocampal network oscillations and theta-gamma coupling arise before Abeta overproduction in a mouse model of Alzheimer's disease. Eur. J. Neurosci. *37*, 1896–1902. https://www.ncbi.nlm.nih.gov/pubmed/23773058.

49. Driver, J.E., Racca, C., Cunningham, M.O., Towers, S.K., Davies, C.H., Whittington, M.A., and LeBeau, F.E. (2007). Impairment of hippocampal gamma-frequency oscillations in vitro in mice overexpressing human amyloid precursor protein (APP). Eur. J. Neurosci. *26*, 1280–1288. https://www.ncbi.nlm.nih.gov/pubmed/17767505.

50. Ittner, A.A., Gladbach, A., Bertz, J., Suh, L.S., and Ittner, L.M. (2014). p38 MAP kinase-mediated NMDA receptor-dependent suppression of hippocampal hypersynchronicity in a mouse model of Alzheimer's disease. Acta Neuropathol. Commun. *2*, 149. https://www.ncbi.nlm.nih.gov/pubmed/25331068.

51. Wang, J., Ikonen, S., Gurevicius, K., van Groen, T., and Tanila, H. (2002). Alteration of cortical EEG in mice carrying mutated human APP transgene. Brain Res. *943*, 181–190. https://www.ncbi.nlm.nih.gov/pubmed/12101040.

52. Donohue, M.C., Sperling, R.A., Petersen, R., Sun, C.K., Weiner, M.W., and Aisen, P.S.; Alzheimer's Disease Neuroimaging Initiative (2017). Association between elevated brain amyloid and subsequent cognitive decline among cognitively normal persons. JAMA *317*, 2305–2316. https://www.ncbi.nlm.nih.gov/pubmed/28609533.

53. Wang, H.W., Pasternak, J.F., Kuo, H., Ristic, H., Lambert, M.P., Chromy, B., Viola, K.L., Klein, W.L., Stine, W.B., Krafft, G.A., et al. (2002). Soluble oligomers of beta amyloid (1–42) inhibit long-term potentiation but not long-term depression in rat dentate gyrus. Brain Res. *924*, 133–140. https://www.ncbi.nlm.nih.gov/pubmed/11750898.

54. Walsh, D.M., and Selkoe, D.J. (2004). Deciphering the molecular basis of memory failure in Alzheimer's disease. Neuron *44*, 181–193. https://www.ncbi.nlm.nih.gov/pubmed/15450169.

55. Selkoe, D.J. (2002). Alzheimer's disease is a synaptic failure. Science *298*, 789–791. https://www.ncbi.nlm.nih.gov/pubmed/12399581.

56. Walsh, D.M., Klyubin, I., Fadeeva, J.V., Cullen, W.K., Anwyl, R., Wolfe, M.S., Rowan, M.J., and Selkoe, D.J. (2002). Naturally secreted oligomers of amyloid beta protein potently inhibit hippocampal long-term potentiation in vivo. Nature *416*, 535–539. https://www.ncbi.nlm.nih.gov/pubmed/11932745.

57. Friedrich, J., Zhou, P., and Paninski, L. (2017). Fast online deconvolution of calcium imaging data. PLoS Comput. Biol. *13*, e1005423. https://www.ncbi.nlm.nih.gov/pubmed/28291787.

58. Pachitariu, M., Stringer, C., and Harris, K.D. (2018). Robustness of spike deconvolution for neuronal calcium imaging. J. Neurosci. *38*, 7976–7985. https://www.ncbi.nlm.nih.gov/pubmed/30082416.

59. Sippy, T., and Yuste, R. (2013). Decorrelating action of inhibition in neocortical networks. J. Neurosci. *33*, 9813–9830. https://www.ncbi.nlm.nih.gov/pubmed/23739978.

60. Stringer, C., and Pachitariu, M. (2019). Computational processing of neural recordings from calcium imaging data. Curr. Opin. Neurobiol. *55*, 22–31. https://www.ncbi.nlm.nih.gov/pubmed/30530255.

61. Vanwalleghem, G., Constantin, L., and Scott, E.K. (2020). Calcium imaging and the curse of negativity. Front. Neural Circuits *14*, 607391. https://www.ncbi.nlm.nih.gov/pubmed/33488363.

62. Tran, C.H., Vaiana, M., Nakuci, J., Somarowthu, A., Goff, K.M., Goldstein, N., Murthy, P., Muldoon, S.F., and Goldberg, E.M. (2020). Interneuron desynchronization precedes seizures in a mouse model of Dravet syndrome. J. Neurosci. *40*, 2764–2775. https://www.ncbi.nlm.nih.gov/pubmed/32102923.

63. Algamal, M., Russ, A.N., Miller, M.R., Hou, S.S., Maci, M., Munting, L.P., Zhao, Q., Gerashchenko, D., Bacskai, B.J., and Kastanenka, K.V. (2022). Reduced excitatory neuron activity and interneuron-type-specific deficits in a mouse model of Alzheimer's disease. Commun. Biol. *5*, 1323. https://www.ncbi.nlm.nih.gov/pubmed/36460716.

64. Kim, N., Li, H.E., Hughes, R.N., Watson, G.D.R., Gallegos, D., West, A.E., Kim, I.H., and Yin, H.H. (2019). A striatal interneuron circuit for continuous target pursuit. Nat. Commun. *10*, 2715. https://www.ncbi.nlm.nih.gov/pubmed/31222009.

65. Oakley, H., Cole, S.L., Logan, S., Maus, E., Shao, P., Craft, J., Guillozet-Bongaarts, A., Ohno, M., Disterhoft, J., Van Eldik, L., et al. (2006). Intraneuronal beta-amyloid aggregates, neurodegeneration, and neuron loss in transgenic mice with five familial Alzheimer's disease mutations: potential factors in amyloid plaque formation. J. Neurosci. *26*, 10129–10140. https://www.ncbi.nlm.nih.gov/pubmed/17021169.

66. Ismeurt, C., Giannoni, P., and Claeysen, S. (2020). The 5xFAD mouse model of Alzheimer's disease. In Diagnosis and Management in Dementia (Elsevier), pp. 207–221.

67. Velasco, E.R., Florido, A., Milad, M.R., and Andero, R. (2019). Sex differences in fear extinction. Neurosci. Biobehav. Rev. *103*, 81–108. https://www.ncbi.nlm.nih.gov/pubmed/31129235.

68. Barker, J.M., and Galea, L.A. (2010). Males show stronger contextual fear conditioning than females after context pre-exposure. Physiol. Behav. *99*, 82–90. https://www.ncbi.nlm.nih.gov/pubmed/19879284.

69. Daviu, N., Andero, R., Armario, A., and Nadal, R. (2014). Sex differences in the behavioural and hypothalamic-pituitary-adrenal response to contextual fear conditioning in rats. Horm. Behav. *66*, 713–723. https://www.ncbi.nlm.nih.gov/pubmed/25311689.

70. Maren, S., De Oca, B., and Fanselow, M.S. (1994). Sex differences in hippocampal long-term potentiation (LTP) and Pavlovian fear conditioning in rats: positive correlation between LTP and contextual learning. Brain Res. *661*, 25–34. https://www.ncbi.nlm.nih.gov/pubmed/7834376.

71. Carrier-Ruiz, A., Sugaya, Y., Kumar, D., Vergara, P., Koyanagi, I., Srinivasan, S., Naoi, T., Kano, M., and Sakaguchi, M. (2021). Calcium imaging of adult-born neurons in freely moving mice. Star Protoc. *2*, 100238. https://www.ncbi.nlm.nih.gov/pubmed/33458703.

72. Resendez, S.L., Jennings, J.H., Ung, R.L., Namboodiri, V.M., Zhou, Z.C., Otis, J.M., Nomura, H., McHenry, J.A., Kosyk, O., and Stuber, G.D. (2016). Visualization of cortical, subcortical and deep brain neural circuit dynamics during naturalistic mammalian behavior with head-mounted microscopes and chronically implanted lenses. Nat. Protoc. *11*, 566–597. https://www.ncbi.nlm.nih.gov/pubmed/26914316.

73. Thévenaz, P., Ruttimann, U.E., and Unser, M. (1998). A pyramid approach to subpixel registration based on intensity. IEEE Trans. Image Process. *7*, 27–41. https://www.ncbi.nlm.nih.gov/pubmed/18267377.

74. Stamatakis, A.M., Resendez, S.L., Chen, K.S., Favero, M., Liang-Guallpa, J., Nassi, J.J., Neufeld, S.Q., Visscher, K., and Ghosh, K.K. (2021). Miniature microscopes for manipulating and recording in vivo brain activity. Microscopy (Oxf) *70*, 399–414. https://www.ncbi.nlm.nih.gov/pubmed/34283242.

75. Pham, J., Cabrera, S.M., Sanchis-Segura, C., and Wood, M.A. (2009). Automated scoring of fear-related behavior using EthoVision software. J. Neurosci. Methods *178*, 323–326. https://www.ncbi.nlm.nih.gov/pubmed/19150629.

76. Jimenez, J.C., Berry, J.E., Lim, S.C., Ong, S.K., Kheirbek, M.A., and Hen, R. (2020). Contextual fear memory retrieval by correlated ensembles of ventral CA1 neurons. Nat. Commun. *11*, 3492. https://www.ncbi.nlm.nih.gov/pubmed/32661319.

77. Kitamura, T., Ogawa, S.K., Roy, D.S., Okuyama, T., Morrissey, M.D., Smith, L.M., Redondo, R.L., and Tonegawa, S. (2017). Engrams and circuits crucial for systems consolidation of a memory. Science *356*, 73–78. https://www.ncbi.nlm.nih.gov/pubmed/28386011.

78. Gründemann, J., Bitterman, Y., Lu, T., Krabbe, S., Grewe, B.F., Schnitzer, M.J., and Lüthi, A. (2019). Amygdala ensembles encode behavioral states. Science *364*, eaav8736. https://www.ncbi.nlm.nih.gov/pubmed/31000636.

79. Besnard, A., Gao, Y., TaeWoo Kim, M., Twarkowski, H., Reed, A.K., Langberg, T., Feng, W., Xu, X., Saur, D., Zweifel, L.S., et al. (2019). Dorsolateral septum somatostatin interneurons gate mobility to calibrate context-specific behavioral fear responses. Nat. Neurosci. *22*, 436–446. https://www.ncbi.nlm.nih.gov/pubmed/30718902.

Please cite this article in press as: Park et al., Memory encoding and retrieval by retrosplenial parvalbumin interneurons are impaired in Alzheimer's disease model mice, Current Biology (2023), https://doi.org/10.1016/j.cub.2023.12.014

CellPress
OPEN ACCESS

STAR★METHODS

KEY RESOURCES TABLE

REAGENT or RESOURCE	SOURCE	IDENTIFIER
Experimental models: Organisms/strains		
PV-Cre mice	Jackson Laboratory	Cat# 017320
5XFAD mice	Jackson Laboratory	Cat# 006554
5XFAD/PV-Cre mice	This paper	N/A
SJL	Jackson Laboratory	Cat# 000686
Bacterial and virus strains		
AAV1-EF1a-DIO-GCaMP6s-P2A-nls-dTomato	Addgene	Cat# 51082
AAV9-Ef1a-DIO-ChR2(E123T/T159C)-eYFP	Addgene	Cat# 35509
AAV5-CaMKII-mCherry	Addgene	Cat# 114469
AAV5-Ef1a-DIO-NpHR3.0-eYFP	Addgene	Cat# 26966
AAV5-Syn-flex-rc[ChrimsonR-tdTomato]	Addgene	Cat# 62723
Antibodies		
Rabbit anti-beta amyloid 1–42	Abcam	Cat# ab201060; RRID: AB_2818982
Donkey anti-rabbit	Jackson ImmunoResearch	Cat# 711-167-003; RRID: AB_2340606
Software and algorithms		
MATLAB R2021a	Mathwork	https://kr.mathworks.com/
Inscopix Data Processing Software	Inscopix	https://iq.inscopix.com/software
Ethovision XT 16	Noldus	https://www.noldus.com/ethovision-xt
Adobe Illustrator 2021	Adobe	https://www.adobe.com/
Igor Pro	WaveMetrics	https://www.wavemetrics.com/downloads/current
Other		
Miniaturized microscope	Inscopix	https://www.inscopix.com/nvoke
GRIN lens	Inscopix	Cat# 1050-004623
Optic cannula	RWD	Cat# 087-00017-00
LED driver	Thorlabs	Cat# LEDD1B

RESOURCE AVAILABILITY

Lead contact

Requests for further information and resources should be directed to and will be fulfilled by the lead contact, Dr. Jeehyun Kwag (jkwag@snu.ac.kr).

Materials availability

This study did not generate new unique reagents.

Data and code availability

All data reported in this paper and the code employed for the analysis will be shared by the lead contact upon request. Any additional information required to reanalyze the data reported in this paper is available from the lead contact upon request.

EXPERIMENTAL MODEL AND SUBJECT DETAILS

Animals

Total two different lines of mice (6 – 9 months old) including the control mice (PV-Cre mice, #017320, Jackson Laboratory, USA) and Alzheimer's disease (AD) mice model (5XFAD/PV-Cre mice[33]) were used with the approval of the Institutional Animal Care and Use Committee (IACUC) at Korea University (KUIACUC-2020-0099, KUIACUC-2021-0052). 5XFAD/PV-Cre (background strain: C57BL/6 x B6SJL F1) mice were generated by crossbreeding of PV-Cre (background strain: C57BL/6) mice and 5XFAD mice[65] (background strain: B6SJL F1) mice (#034840, Jackson Laboratory, USA), following the a previous study that used 5XFAD/PV-Cre mice.[33] 5XFAD

Please cite this article in press as: Park et al., Memory encoding and retrieval by retrosplenial parvalbumin interneurons are impaired in Alzheimer's disease model mice, Current Biology (2023), https://doi.org/10.1016/j.cub.2023.12.014

mice were backcrossed on B6SJL F1 (C57BL/6 x SJL) background to keep their phenotype pronounce.[66] All mice were individually housed in a temperature- and humidity-controlled vivarium, which was kept in a 12 h/12 h light/dark cycle. All experiments were performed during the dark cycle. Food and water were available ad libitum. Only male mice were used throughout this study as male and female rodents have been reported to exhibit different freezing behaviors in response to electrical foot shocks during contextual fear memory task.[67–70]

METHOD DETAILS

Virus and stereotaxic surgery for *in vivo* Ca^{2+} imaging

For surgical procedure, mice were deeply anesthetized using 2% isoflurane (2 ml/min flow rate) and head-fixed into a stereotaxic frame (51730D, Stoelting Co., USA). For *in vivo* Ca^{2+} imaging of PV interneurons from PV-Cre or 5XFAD/PV-Cre mice (Figures 1, 2, and S1–S4), AAV1-EF1a-DIO-GCaMP6s-P2A-nls-dTomato (#51082, Addgene, USA) in solution (5 x 10^{12} virus molecules/ml diluted with saline at 1:1 ratio) was used. Virus was injected into three sites (500 nl per injection site) along the dorsoventral axis of the retrosplenial cortex (RSC) (AP: –2.5 mm, ML: –0.3 mm, DV: –0.8, –0.6, and –0.4 mm) using a Hamilton syringe (#87930, Hamilton, USA) controlled by an automated stereotaxic injector (100 nl/min; #53311, Stoelting Quintessential Injector, Stoelting Co., USA). The syringe was left at the injection coordinates for more than 5 min to allow viral diffusion.

After viral injection, a Gradient-index (GRIN) lens (1 mm diameter, 4 mm length; #1050-004605, Inscopix, USA) was implanted to RSC (AP: –2.5 mm; ML: –0.3 mm; DV: –0.5 mm) by lowering the lens in 100 μm steps (0.2 mm/min) to allow the brain tissue to settle and to avoid damaging the tissue.[71] After reaching the target coordinate, GRIN lens was fixed to the skull with dental cement (Self Curing, Vertex, Netherlands). After two weeks of recovery time following the surgery, mice were deeply anesthetized using 2% isoflurane (2 ml/min flow rate) to attach a magnetic baseplate (#1050-004638, Inscopix, USA), on top of which a miniaturized microscope (nVoke, Inscopix, USA) was mounted. If GCaMP6s-expressing neurons were visible in the field of view (FOV), the baseplate was fixed to the skull using dental adhesive resin cement (Super bond, Sun Medical, Japan) to perform *in vivo* longitudinal Ca^{2+} imaging of the same FOV. After baseplating, at least one week of recovery time was allowed before performing *in vivo* Ca^{2+} imaging.

Virus and stereotaxic surgery for *in vitro* optogenetic experiments

For *in vitro* optogenetic stimulation of PV interneurons from PV-Cre or 5XFAD/PV-Cre mice (Figure 3), both AAV9-Ef1a-DIO-ChR2(E123T/T159C)-eYFP (#35509, Addgene, USA) in solution (1 x 10^{13} virus molecules/ml diluted with saline at 3:1 ratio) and AAV5-CaMKII-mCherry (#114469, Addgene, USA) in solution (7 x 10^{12} virus molecules/ml diluted with saline at 3:1 ratio) were used following the same virus injection protocols for *in vivo* Ca^{2+} imaging. After viral injection, at least two weeks of recovery time was allowed before performing *in vitro* optogenetic experiments.

Virus and stereotaxic surgery for *in vivo* optogenetic experiments

For *in vivo* optogenetic inactivation/activation of PV interneurons from PV-Cre or 5XFAD/PV-Cre mice (Figure 4), AAV5-Ef1a-DIO-NpHR3.0-eYFP (#26966, Addgene, USA) in solution (1 x 10^{13} virus molecules/ml diluted with saline at 3:1 ratio) or AAV5-Syn-flex-rc[ChrimsonR-tdTomato] (#62723, Addgene, USA) in solution (5 x 10^{12} virus molecules/ml diluted with saline at 3:1 ratio) were used, respectively, following the same virus injection protocols for *in vivo* Ca^{2+} imaging with slight modification of injection site (AP: 2.5 mm, ML: ± 0.3 mm, DV: –0.8, –0.6, and –0.4 mm). After viral injection, two optic cannulas (400 μm core diameter, 2 mm length; #087-00017-00, RWD, China) were implanted to both right and left RSC (AP: ±2.5 mm; ML: –0.3 mm; DV: –0.5 mm) and fixed to the skull with dental cement (Self Curing, Vertex, Netherlands). After optic fiber implant, at least two week of recovery time was allowed before performing *in vivo* optogenetic experiments.

In vivo Ca^{2+} imaging and signal processing

Prior to *in vivo* Ca^{2+} imaging during behavior task, mice were adapted to the head-mounted miniaturized microscope connected to the commutator systems (Inscopix, USA) for at least five days. All experiments were performed under the luminescence of 30 Lux.

In vivo Ca^{2+} imaging data from GCaMP6s-expressing RSC neurons were acquired using nVoke acquisition software (Inscopix, USA) at a sampling rate of 20 Hz (exposure time: 50 ms). An optimal LED power (0.1 – 0.7 mW/mm^2) and digital focus (0 – 1000) was selected for each mouse based on GCaMP6s expression in neurons in the FOV and the same parameters were used for each mouse for longitudinal imaging.

Ca^{2+} image processing was performed using Inscopix Data Processing Software (Inscopix, USA), following other studies.[60,72] For all data, motion correction was applied using an image registration method.[72,73] Mean fluorescence signal value (F) of each pixel across the entire Ca^{2+} image video was used to calculate the reference, termed F_0. Then, changes in fluorescence signal value ($\triangle F$) of each pixel were normalized by F_0 to acquire $\triangle F/F_0$. Putative neurons and their Ca^{2+} signals were isolated using automated cell-segmentation algorithm on $\triangle F/F_0$ data, which is based on principal component analysis-independent component analysis.[72,74]

Putative spikes were inferred from $\triangle F/F_0$ signal using spike deconvolution algorithm called "Online Active Set methods to Infer Spikes"[57–60]. Spikes with an amplitude less than 3 signals-to-noise ratio of deconvolved Ca^{2+} signals were removed from the data. Ca^{2+} transient (Figures S2 and S4) were defined using Ca^{2+} event detection algorithm which detects the large amplitude peaks (3 standard deviation (sd) from $\triangle F/F_0$ signal) with slow decays (minimum: 0.2 s) by thresholding at the local maxima of the $\triangle F/F_0$.

Please cite this article in press as: Park et al., Memory encoding and retrieval by retrosplenial parvalbumin interneurons are impaired in Alzheimer's disease model mice, Current Biology (2023), https://doi.org/10.1016/j.cub.2023.12.014

To investigate the baseline activity of PV interneurons (Figure S1), inter-spike frequencies were analyzed by calculating the intervals between all consecutive spikes of PV interneurons from either PV-Cre or 5XFAD/PV-Cre mice. Inter-spike frequencies of up to 20 Hz were analyzed due to the sample rate of Ca^{2+} imaging (20 Hz). Based on the PV interneuron's inter-spike frequencies, probability distributions and cumulative probability distributions were plotted.

Contextual fear memory task

Contextual fear memory task[24] was performed in a rectangular shaped conditioning chamber (width: 30 cm, length: 26 cm, height: 33 cm, Coulbourn Instruments, USA) with stainless-steel grid floor composed of 16 grid bars. The grid floor was connected to a precision animal shocker (Coulbourn Instruments, USA) set to deliver electrical foot shocks (0.5 mA, 1 s-long). On the first day of contextual fear memory task (habituation), mice were habituated in the conditioning chamber for 3 min. On the second day, mice were placed in the same chamber for contextual fear conditioning, consisting of 120 s pre-stimulus period followed by delivery of three aversive electric foot shocks (120 s inter-stimulus intervals) to form associative memory between the context of the chamber and the electric foot shocks. On the last day, mice were returned to the same chamber for 3 min without the delivery of electric foot shocks to assess contextual fear memory retrieval, measured as freezing behavior. Freezing behavior was defined based on the immobility of mice which was captured by detecting the time epochs showing the video pixels of a detected mouse between the behavior data sample points less than threshold (0.5%–3%).[75] The threshold of video pixel change for each mouse was decided based on the visual inspection. For experiments with naïve mice (Figure 3), mice were subjected to the same contextual fear memory task over three days but without receiving any electric foot shocks during conditioning sessions.

For *in vivo* optogenetic stimulation of PV interneurons during contextual fear memory task (Figure 4), optic cannulas were connected to an LED driver (T-Cube™ LED driver, Thorlabs, USA) via patch cables connected to a FC/PC rotary joint (RJ1, Thorlabs, USA). Mice were adapted to the attached patch cables at least five days before contextual fear memory task. During the whole contextual fear memory task, patch cables were attached and 595 nm yellow light stimulations (3 s-long) were delivered 1 s preceding each electrical foot shock to optogenetically stimulate PV interneurons during conditioning. Light intensity was set to output 5 mW at the tip of the optic fibers.

After each session of the contextual fear memory task, the conditioning chamber was cleaned using 70% ethanol to eliminate any odors. Mice behavior was recorded by a video camera placed on the ceiling above the chambers or arenas at a sampling rate of 7.5 Hz. All behavior data including video pixel changes and velocity were analyzed using Ethovision XT 16 program (Noldus, Netherlands).

Histology and immunohistochemistry

To confirm the position of GRIN lens track or optic fiber track and viral expression in granular RSC PV interneurons after Ca^{2+} imaging or *in vivo* optogenetic experiments, the brain was removed from the mice that were deeply anesthetized using Avertin (8 g of 2, 2, 2-Tribromoethanol and 5.1 ml of 2-methyl-2-butanol in 402.9 ml saline, Sigma Aldrich, USA) at a delivery rate of 0.2 ml/10 g body weight and perfused with 10 ml chilled 4% paraformaldehyde (PFA, 158127, Sigma-Aldrich, USA) transcardially. The brain was fixed overnight in 4% paraformaldehyde and transferred to 30% sucrose solution in phosphate-buffered saline (PBS) for cryoprotection for 24 – 48 h. Brains were frozen in Optimum Cutting Temperature (OCT) compounds (Tissue-Tek O.C.T. Compound, SAKURA, Japan) at –50°C prior to cryosectioning in 100 μm-thick coronal slices on a cryostat (YD-2235, Jinhua Yidi Medical Appliance Co., China). Slices were washed three times with PBS to wash out the OCT compounds and mounted on slide glasses with an antifade mounting medium with DAPI (Vectashield, Vector Laboratories, USA). Ca^{2+} imaging locations or *in vivo* optogenetic stimulation locations were identified based on the position of GRIN lens track or optic fiber track, respectively. Expression of virus on PV interneurons was verified by detecting the fluorescent signal using a confocal microscope (LSM-700, ZEISS, Germany) and fluorescent microscope (DM2500, Leica, Germany).

To verify the deposition of beta-amyloid (Aβ) on the RSC area of brain slices from 5XFAD/PV-Cre mice, PFA-fixed brain slices were incubated in peroxidase buffer (0.3% H_2O_2 in 0.1 M PBS) for 20 min. Non-targeted antigens were blocked by incubation in 6% bovine serum albumin and 0.3% Triton X-100 in 0.1 M PBS for > 24 h at 4 °C, after which slices were incubated with primary anti-Aβ antibody (1:300 dilution in 0.1 M PBS, at 4 °C for 4 days)(anti-Aβ 1–42 antibody [mOC64]-Conformation-Specifc, #ab201060, Abcam, UK) and secondary antibody (1:500 dilution in 0.1 M PBS)(CyTM3 AfniPure Donkey Anti-Rabbit IgG (H +L), Jackson ImmunoResearch, USA). Slices were washed three times with PBS and mounted on slide glasses with an antifade mounting medium. Deposition of Aβ was verified by detecting the fluorescent signal using a confocal microscope (LSM-700, ZEISS, Germany) and fluorescent microscope (DM2500, Leica, Germany).

Neural selectivity analysis

Ca^{2+} imaging data from Inscopix and behavior data from Ethovision XT 16 were synchronized using Noldus-IO box (Mini USB-IO box, Noldus, Netherlands) system, which were then analyzed with custom-made Matlab (Mathworks, USA) code. To analyze the responsiveness of RSC PV interneurons to contextual fear conditioning-inducing electric foot shocks[76,77] (Figures 1 and S2), their spike firing rates in response to electrical foot shocks (shock response) in the time windows of 0 s to 3 s at the onset of electrical foot shock delivery were calculated. A neuron was defined as shock-responsive (shock-R) if the shock response exceeded the 95th percentile of randomly shuffled shock response distribution of each single neuron. Shuffled shock response distribution was generated by circularly time-shifting the spike trains of neurons with randomly selected period along the mouse behavior data with 1000 repetitions

Please cite this article in press as: Park et al., Memory encoding and retrieval by retrosplenial parvalbumin interneurons are impaired in Alzheimer's disease model mice, Current Biology (2023), https://doi.org/10.1016/j.cub.2023.12.014

following the method used in previous studies.[78] This random time-shuffling preserved the temporal structures of both Ca^{2+} signals and behavior data while disrupting the temporal correlation between them. Random time-shuffling was applied for all randomly shuffled distribution for other metric.

To analyze ensemble dynamics of RSC PV interneurons during freezing and unfreezing epochs[78,79] (Figures 2, S3, and S4), their neuronal firing rates were Z-scored in the time windows of -2 s to 4 s at the onset of freezing or unfreezing epochs.[78] Time window of -2 to 0 s at the freezing or unfreezing epochs were used as baseline periods for Z-scored analysis. A neuron was defined as upregulated if the mean Z-score of the neuronal activity during freezing or unfreezing epochs exceeded the 95th percentile of randomly shuffled Z-score distributions of each single neuron, respectively. On the other hand, a neuron was defined as suppressed if the mean Z-score of the neuronal activity during freezing or unfreezing epochs fell below the 5th percentile of randomly shuffled Z-score distributions of each single neuron, respectively. Other neurons were defined as non-selective to freezing or unfreezing epochs.

In vitro RSC slice preparation

Mice were deeply anesthetized using 1.25% Avertin solution at a delivery rate of 0.2 ml/10 g body weight and perfused with ice-cold cutting solution (containing (in mM): 180 sucrose, 2.5 KCl, 1.25 NaH_2PO_4, 25 $NaHCO_3$, 11 glucose, 2 $MgSO_4$, and 1 $CaCl_2$ at pH 7.2–7.4 oxygenated with 95% O_2/5% CO_2). Coronal RSC slices (300 μm) were cut using a vibratome (VT 1000 S, Leica Microsystems, Germany). Slices were allowed to recover for 30 min in a mixture of cutting solution and artificial cerebrospinal fluid (aCSF, containing (in mM): 126 NaCl, 3 KCl, 1.25 NaH_2PO_4, 2 $MgSO_4$, 2 $CaCl_2$, 25 $NaHCO_3$, and 10 glucose at pH 7.2–7.4 bubbled with 95% O_2/5% CO_2) solution at 1:1 ratio, after which the slices were further incubated in aCSF for at least 1 h at 30–32 °C before performing *in vitro* electrophysiological recordings.

In vitro whole-cell patch-clamp recordings

Slices were moved to a recording chamber filled with aCSF (30–32 °C), and RSC area was identified under the guidance of differential interference contrast microscopy (BW51W, Olympus). To perform *in vitro* optogenetic light stimulation (Figure 3), 470 nm blue light (X-Cite, Excelitas Technologies, USA) was delivered through the objective (x 40) of the microscope (BX51W, Olympus, Japan) which covered the 550 μm diameter circle of the RSC area with the center of the illumination positioned at the patch clamp electrode. To record PV interneuron-evoked inhibitory postsynaptic currents from excitatory neurons, channelrhodopsin-2 (ChR2)-expressing RSC PV interneurons were optically stimulated with 470 nm blue light in PV-Cre or 5XFAD/PV-Cre mice, while whole-cell voltage-clamp recordings were made from RSC excitatory neurons using borosilicate glass electrode (4–8 MΩ) filled with internal solution containing (in mM) 115 Cesium methanesulfonate (CsMSF), 8 NaCl, 10 HEPES, 0.3 GTP-NaCl, 4 ATP-Mg, 0.3 EGTA, 5 QX-314, and 10 BAPTA (pH 7.3–7.4 and 280–290 mOsm/L). IPSC was recorded at the holding potential of 10 mV. To analyze the stimulus-response (S-R) curve of PV interneuron-evoked IPSC (Figures 3B and 3C), a single 470 nm blue light pulse (1 ms) with different stimulation intensities (5, 10, 15, 20, and 30 % of maximal light power (15 mW))[1,2] was delivered to ChR2-expressing PV interneurons and the corresponding evoked IPSCs were recorded from RSC excitatory neurons. For the subsequent paired-pulse ratio (PPR) analysis (Figures 3D and 3E), two 470 nm blue light pulses (1 ms) with stimulation intensity that gave the half-maximal IPSC response in the S-R curve[1,2] were delivered at 20 Hz. PPR was calculated by normalizing the amplitude of second evoked IPSC by that of first evoked-IPSC. All signals were amplified (MultiClamp 700B amplifier, Molecular Devices, USA), low-pass filtered at 10 kHz, and acquired at 5 kHz using the ITC-18 data acquisition interface (HEKA Elektronik, Germany). Igor Pro software (WaveMetrics, USA) was used for generating command signals and acquiring data after which acquired data were then analyzed with custom-made Matlab code.

QUANTIFICATION AND STATISTICAL ANALYSIS

Statistics

Data are represented as mean ± SEM. Statistical significance was measured using paired or unpaired Student's t test, one-way, two-way, or three-way ANOVA with post hoc Tukey's test, and permutation test.

Current Biology, Volume *34*

Supplemental Information

Memory encoding and retrieval by retrosplenial parvalbumin interneurons are impaired in Alzheimer's disease model mice

Kyerl Park, Michael M. Kohl, and Jeehyun Kwag

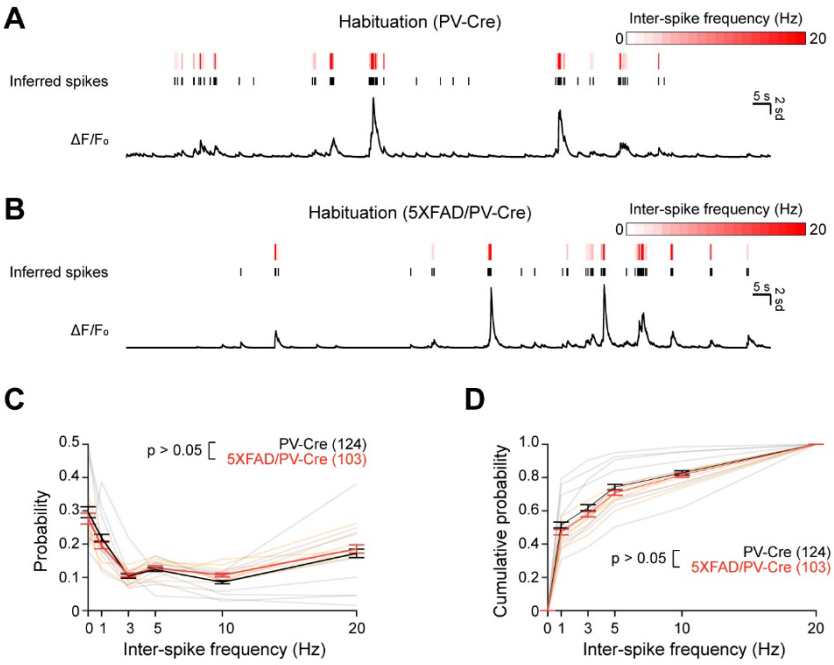

Figure S1. Inter-spike frequency analysis of deconvoluted spikes of PV interneurons in granular retrosplenial cortex of PV-Cre and 5XFAD/PV-Cre mice. Related to Figure 1.

(**A, B**) Representative raw Ca^{2+} signals ($\triangle F/F_0$) of a single PV interneuron in the granular retrosplenial cortex (RSC) of PV-Cre mouse (A) or 5XFAD/PV-Cre mouse (B) during habituation session, from which deconvoluted spikes (inferred spikes) were extracted to analyze inter-spike frequencies. (**C**) Probability distributions of inter-spike frequencies of PV interneurons from PV-Cre and 5XFAD/PV-Cre mice during habituation session [Two-way ANOVA with post hoc Tukey's test, Two-way interaction, $F(5, 1350) = 1.52$, $p = 0.18$]. Gray lines and orange lines indicate the individual mouse data of PV-Cre and 5XFAD/PV-Cre mice, respectively. (**D**) Cumulative probability plot of inter-spike frequencies of deconvoluted spikes of PV interneurons from PV-Cre and 5XFAD/PV-Cre mice during habituation session [Two-way ANOVA with post hoc Tukey's test, Two-way interaction, $F(5, 1350) = 1.16$, $p = 0.33$]. Gray lines and orange lines indicate the individual mouse data of PV-Cre and 5XFAD/PV-Cre mice, respectively. Data are represented as mean ± SEM.

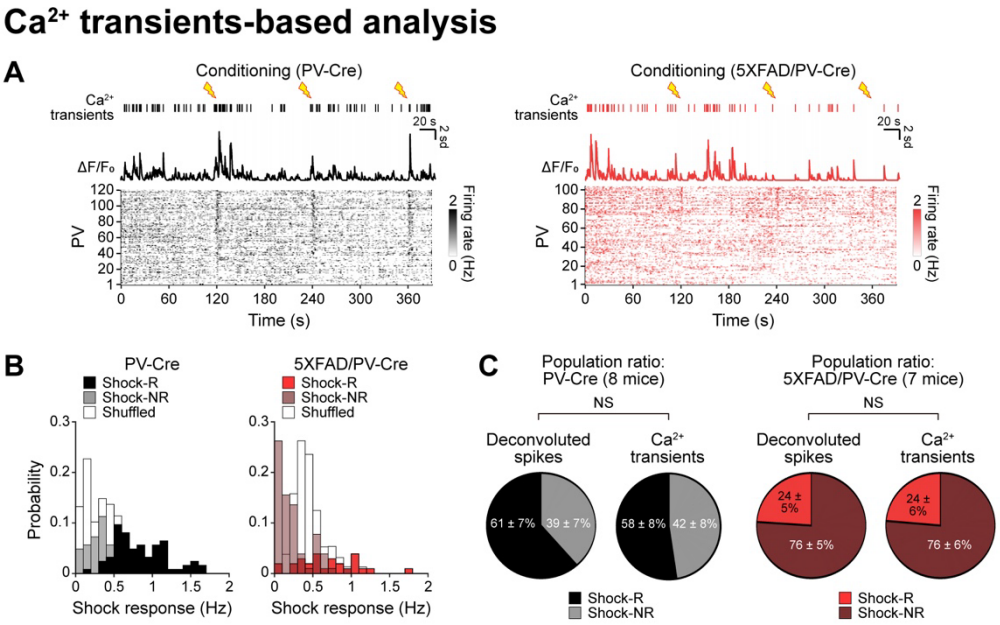

Figure S2. Ca^{2+} transients-based analysis of shock responsiveness of PV interneurons in the granular retrosplenial cortex in PV-Cre and 5XFAD/PV-Cre mice. Related to Figure 1.

(**A**) Representative raw Ca^{2+} signals ($\triangle F/F_o$) recorded from a PV interneuron in the granular retrosplenial cortex (RSC) during contextual fear conditioning session of PV-Cre mouse (black) and 5XFAD/PV-Cre mouse (red) (top), from which Ca^{2+} transients were extracted to plot RSC neuronal Ca^{2+} transient (event) firing rate map of all imaged PV interneurons (bottom). Data from the same PV-Cre and 5XFAD/PV-Cre mouse used in plotting Figure 1E is represented for direct comparison with deconvoluted spikes. (**B**) Probability distributions of Ca^{2+} transient (event) firing rate of shock-responsive (shock-R) and shock non-responsive (shock-NR) PV interneurons from PV-Cre mice or 5XFAD/PV-Cre mice in response to electric foot shocks (shock response) plotted together with the randomly shuffled shock response for comparison (white). (**C**) Pie chart showing population ratio of shock-R and shock-NR PV interneurons analyzed based on either spike deconvolution methods or Ca^{2+} transients-based methods [Unpaired Student's t test, deconvoluted spikes *vs* Ca^{2+} transients, PV-Cre, Shock-R, $t(14) = 0.29$, $p = 0.78$; PV-Cre, Shock-NR, $t(14) = -0.29$, $p = 0.78$; 5XFAD/PV-Cre, Shock-R, $t(12) = 0.04$, $p = 0.97$; 5XFAD/PV-Cre, Shock-NR, $t(12) = -0.04$, $p = 0.97$]. Data are represented as mean ± SEM. NS: $p > 0.05$ for unpaired Student's t test (C).

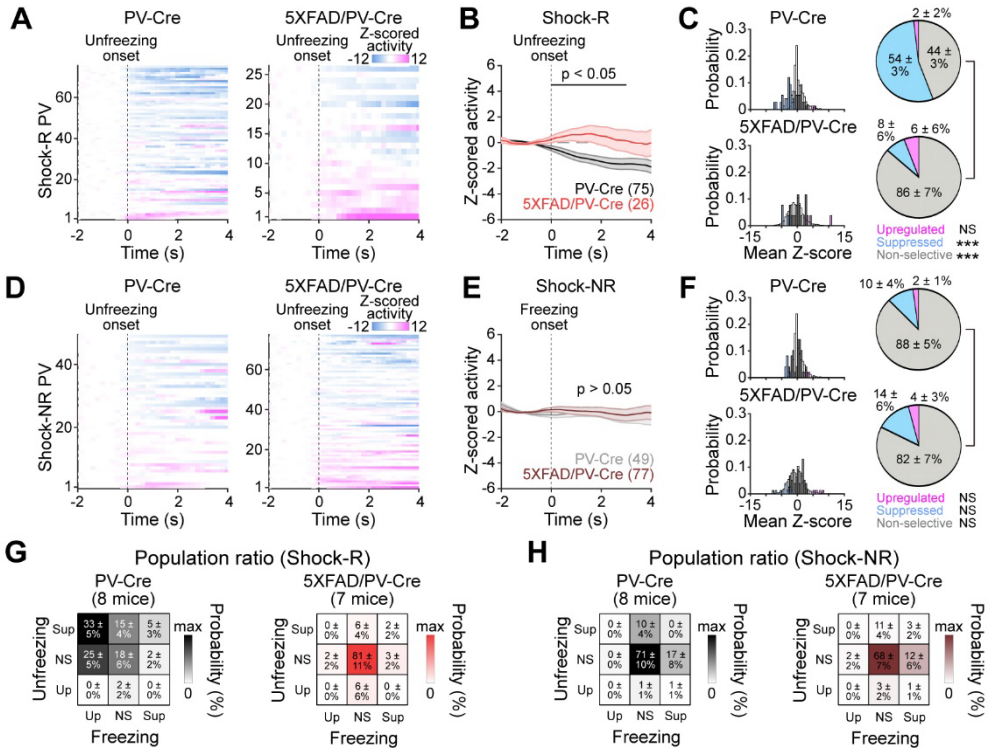

Figure S3. Selective suppression of contextual fear memory-encoding PV interneuron ensemble dynamics in the granular retrosplenial cortex during unfreezing epoch of memory retrieval is disrupted in 5XFAD/PV-Cre mice. Related to Figure 2.

(**A**) Z-scored neuronal activity map of shock-responsive (shock-R) PV interneurons in the granular retrosplenial cortex at the onset of unfreezing epoch in PV-Cre (left) and 5XFAD/PV-Cre mice (right). (**B**) Averaged Z-scored neuronal activities of shock-R PV interneuron at the onset of unfreezing epoch in PV-Cre mice (black) and 5XFAD/PV-Cre mice (red). Solid line: mean Z-scored activity. Shade: SEM. Black horizontal line: significant differences according to the Permutation test. (**C**) Probability distributions (left) of mean Z-score of neuronal activities of shock-R PV interneurons during freezing epoch plotted together with the randomly shuffled mean Z-score for comparison (white). Population ratio (right) of upregulated, suppressed, and non-selective shock-R PV interneuron according to the mean Z-score at the onset of unfreezing epoch [Unpaired Student's t test, PV-Cre *vs* 5XFAD/PV-Cre, Upregulated, $t(13) = -0.70$, $p = 0.50$; Suppressed, $t(13) = 6.93$, $p < 0.001$; Non-selective, $t(13) = -5.59$, $p < 0.001$]. (**D-F**) Same with (A-C) but for shock non-responsive (shock-NR) interneurons from PV-Cre mice or 5XFAD/PV-Cre mice. (**G**, **H**) Population ratio of upregulated (Up), non-selective (NS), and suppressed (Sup) shock-R (G) and shock-NR (H) PV interneurons according to the mean Z-score at the onset of

freezing and unfreezing epochs. Permutation test (B, E). ***$p < 0.001$, NS: $p > 0.05$ for unpaired Student's t test (C, F).

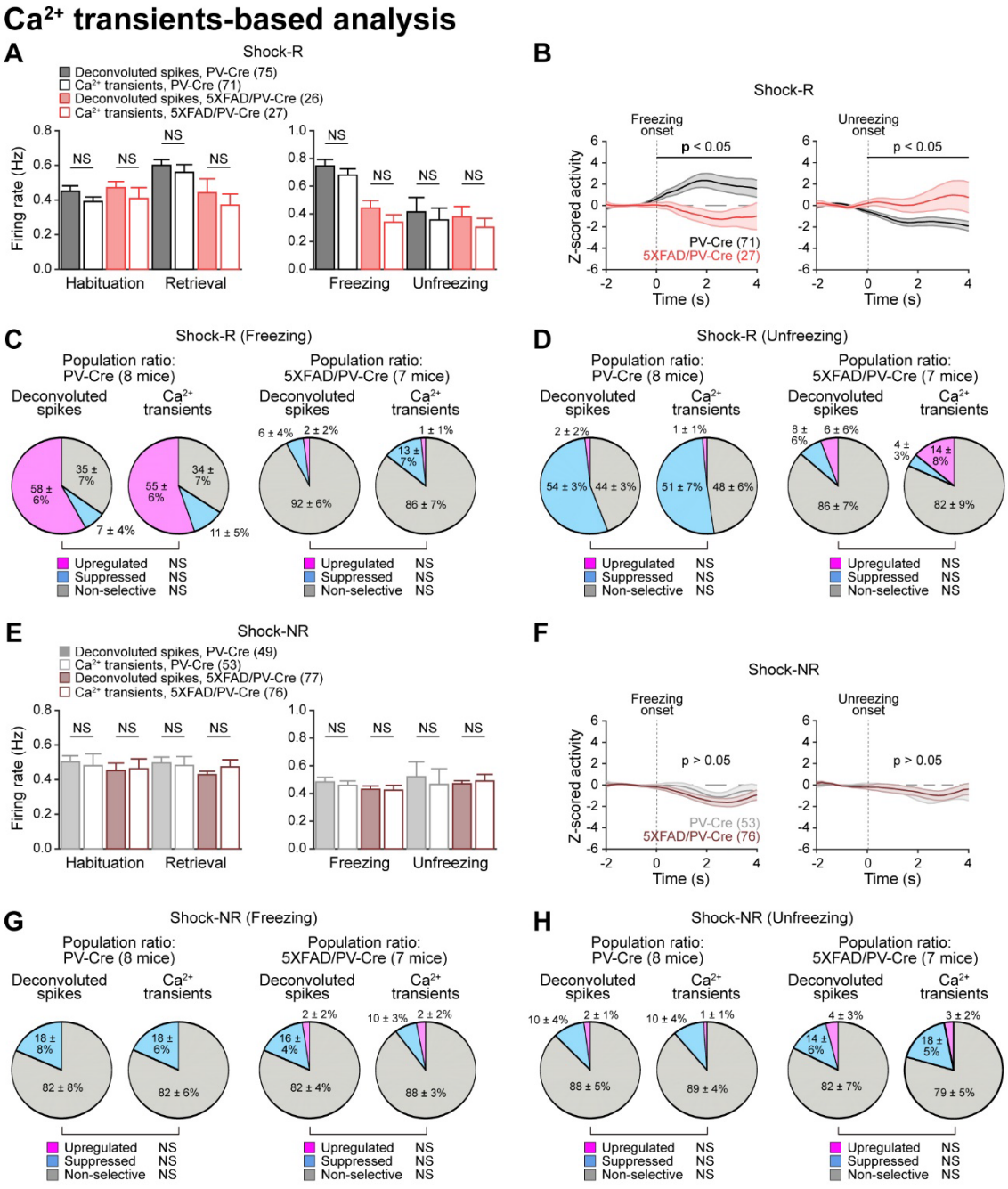

Figure S4. Ca^{2+} transients-based analysis of freezing/unfreezing-selective ensemble dynamics of shock-responsive PV interneuron in the granular retrosplenial cortex. Related to Figure 2.

(**A**) Comparison between averaged firing rates of deconvoluted spikes and Ca^{2+} transients of shock-responsive (shock-R) PV interneurons during habituation and retrieval sessions of contextual fear memory task [Unpaired Student's t test, Habituation, PV-Cre, p = 0.16; 5XFAD/PV-Cre, p = 0.40; Retrieval, PV-Cre, p = 0.47; 5XFAD/PV-Cre, p = 0.49; Freezing, PV-Cre: p = 0.31; 5XFAD/PV-Cre, p = 0.18; Unfreezing, PV-Cre, p = 0.67; 5XFAD/PV-Cre, p =

0.45]. (**B**) Averaged Z-scored Ca^{2+} transients-based neuronal activities of shock-R PV interneuron at the onset of either freezing or unfreezing epoch. Solid line: mean Z-scored activity. Shade: SEM. Black horizontal line: significant differences according to the Permutation test. (**C**, **D**) Comparison between deconvoluted spike-based and Ca^{2+} transients-based pie chart showing population ratio of upregulated, suppressed, and non-selective shock-R PV interneuron according to the mean Z-score at the onset of freezing (C) [Unpaired Student's t test, deconvoluted spikes *vs* Ca^{2+} transients, PV-Cre, Upregulated, p = 0.75; Suppressed, p = 0.61; Non-selective, p = 0.95; 5XFAD/PV-Cre, Upregulated, p = 0.84; Suppressed, p = 0.43; Non-selective, p = 0.53] or unfreezing epoch (D) [Unpaired Student's t test, deconvoluted spikes *vs* Ca^{2+} transients, PV-Cre, Upregulated, p = 0.89; Suppressed, p = 0.69; Non-selective, p = 0.64; 5XFAD/PV-Cre, Upregulated, p = 0.45; Suppressed, p = 0.59; Non-selective, p = 0.84]. (**E**-**H**) Same for (A-D), but for shock non-responsive (shock-NR) PV interneurons [(E), Unpaired Student's t test, Habituation, PV-Cre, p = 0.78; 5XFAD/PV-Cre, p = 0.88; Retrieval, PV-Cre, p = 0.82; 5XFAD/PV-Cre, p = 0.32, Freezing, PV-Cre, p = 0.61; 5XFAD/PV-Cre, p = 0.86; Unfreezing, PV-Cre, p = 0.73, 5XFAD/PV-Cre, p = 0.70] [(G), Unpaired Student's t test, deconvoluted spikes *vs* Ca^{2+} transients, PV-Cre, Upregulated, p = 1; Suppressed, p = 0.98; Non-selective, p = 0.98; 5XFAD/PV-Cre, Upregulated, p = 0.79; Suppressed, p = 0.23; Non-selective, p = 0.25] [(H), Unpaired Student's t test, deconvoluted spikes *vs* Ca^{2+} transients, PV-Cre, Upregulated, p = 0.59; Suppressed, p = 0.98; Non-selective, p = 0.87; 5XFAD/PV-Cre, Upregulated, p = 0.81; Suppressed, p = 0.60; Non-selective, p = 0.69]. NS: $p > 0.05$ for unpaired Student's t test (A, C, D, E, G, H). Permutation test (B, F).